Naval Research Laboratory

Washington, DC 20375-5320

NRL/MR/6410--96-7859

Direct Simulation Monte Carlo Study of H/H_2 and $H/H_2/CO$ Mixtures for Diamond Chemical Vapor Deposition

ROBERT S. SINKOVITS

Center for Reactive Flow and Dynamical Systems
Laboratory for Computational Physics & Fluid Dynamics

C. RICHARD DEVORE

Center for Computational Physics Developments
Laboratory for Computational Physics & Fluid Dynamics

June 13, 1996

REPORT DOCUMENTATION PAGE

Form Approved
OMB No. 0704-0188

1. AGENCY USE ONLY (*Leave Blank*)	2. REPORT DATE	3. REPORT TYPE AND DATES COVERED
	June 13, 1996	

4. TITLE AND SUBTITLE

Direct Simulation Monte Carlo Study of H/H_2 and $H/H_2/CO$ Mixtures for Diamond Chemical Vapor Deposition

5. FUNDING NUMBERS

64-3780-A-6
62712E

6. AUTHOR(S)

Robert S. Sinkovits and C. Richard DeVore

7. PERFORMING ORGANIZATION NAME(S) AND ADDRESS(ES)

Naval Research Laboratory
Washington, DC 20375-5320

8. PERFORMING ORGANIZATION REPORT NUMBER

NRL/MR/6410--96-7859

9. SPONSORING/MONITORING AGENCY NAME(S) AND ADDRESS(ES)

Advanced Research Projects Agency
3701 North Fairfax Drive
Arlington, VA 22203-1714

10. SPONSORING/MONITORING AGENCY REPORT NUMBER

11. SUPPLEMENTARY NOTES

12a. DISTRIBUTION/AVAILABILITY STATEMENT

Approved for public release; distribution unlimited.

12b. DISTRIBUTION CODE

13. ABSTRACT (*Maximum 200 words*)

One-dimensional direct simulation Monte Carlo calculations have been carried out on H/H_2 and $H/H_2/CO$ mixtures under operating conditions typical of diffusion-dominated diamond chemical vapor deposition processes. Mechanisms have been included in the model for the adsorption and recombination of hydrogen atoms on the diamond surface and the dissociation of molecular hydrogen at the interior of the reactor. Hydrogen atom fluxes and recombinative and conductive heat fluxes to the diamond surface are calculated as a function of pressure, gas composition, hydrogen dissociation and surface reaction probabilities, reactor temperature, and distance between the activating source and substrate. The numerical calculations are shown to be in excellent agreement with analytical results in the limiting regimes of free-streaming particles at low pressures and continuum hydrodynamics at high pressures.

14. SUBJECT TERMS

Diamond growth
Chemical kinetics
Chemical vapor deposition

15. NUMBER OF PAGES

57

16. PRICE CODE

17. SECURITY CLASSIFICATION OF REPORT	18. SECURITY CLASSIFICATION OF THIS PAGE	19. SECURITY CLASSIFICATION OF ABSTRACT	20. LIMITATION OF ABSTRACT
UNCLASSIFIED	UNCLASSIFIED	UNCLASSIFIED	UL

NSN 7540-01-280-5500

Standard Form 298 (Rev. 2-89)
Prescribed by ANSI Std 239-18
298-102

CONTENTS

DIRECT SIMULATION MONTE CARLO STUDY OF H/H_2 AND $H/H_2/CO$ MIXTURES FOR DIAMOND CHEMICAL VAPOR DEPOSITION

I. INTRODUCTION

Chemical vapor deposition (CVD) has become the dominant technique for the growth of high-quality diamond films possessing exceptional mechanical, optical, thermal, and electrical properties [1]. Successful diamond growth has been demonstrated over a wide range of conditions using microwave plasma, hot filament, combustion flame, and plasma torch reactors. These various techniques can be classified as either diffusion-dominated or convection-dominated on the basis of their characteristic Peclet number [2], defined as $Pe = uL/D$, where D is the diffusion coefficient, u is the flow velocity, and L is the length scale for the transport of species to the diamond surface. The microwave plasma and hot filament reactors typically involve very slow flow velocities and fall well within the diffusion dominated regime ($Pe \ll 1$), while the combustion flame and plasma torch reactors, which rely on the high-speed forced convection of gases to the diamond surface, are clearly convection-dominated ($Pe \gg 1$).

The focus of this paper is on the diffusion-dominated processes. In this regime, convective gas flow can be neglected and the problem can be effectively reduced to that of diffusion through a one-dimensional boundary layer. To study this system, we use the direct simulation Monte Carlo (DSMC) method [3]. This approach allows us to accurately extend our calculations over a range of conditions from those where a Navier-Stokes continuum treatment is valid into a regime where rarefied gas effects are important. Since DSMC is a particle based method, the effects of molecular diffusion, thermal diffusion, viscosity, and thermal conduction are all implicitly treated.

The primary aim of this work is to determine the effects of the operating condi-

Manuscript approved May 6, 1996.

tions on the hydrogen-atom and thermal fluxes to the substrate. A number of studies have shown the critical role of hydrogen atoms in both creating, through hydrogen abstraction reactions, surface radical sites where growth species can be added [4, 5], and in "annealing" the surface by promoting sp^3 bonding among carbon atoms newly added to the diamond lattice [4, 6]. Since we are not here concerned with the specific mechanisms of carbon addition, simplifications can be made concerning the composition of the gas phase.

Standard diamond CVD source gas recipes consist of a small amount (≤ 1 %) of methane in hydrogen. The relatively small concentrations of methane, methyl radicals, and other carbon species will have negligible effects on the thermal conductivity of the mixture and the diffusion of atomic and molecular hydrogen. Such mixtures can be approximated in our present simulations as pure hydrogen. Similar simplifying assumptions can be made for source gases containing oxygen. Bachmann *et al.* [7] have shown that source gas recipes containing oxygen can be categorized as leading to diamond growth, non-diamond growth, or no growth based solely on their overall C-H-O stoichiometry. This independence of the particular source gases employed suggests that a quasi-thermodynamic equilibrium is established before the gases reach the diamond surface. Consequently, the carbon and oxygen in the system will react to form as much carbon monoxide as possible, leaving the excess element to form either growth (CH_3, C, etc.) or etching (OH, O) species. Since the highest quality diamond growth occurs for mixtures with only a small excess of carbon to oxygen, it is reasonable to model these systems, for the purpose of this study, as $H/H_2/CO$ mixtures. Because of our interest in diamond growth from ethanol-water source gases [8–11], we have chosen an $H/H_2/CO$ mixture with a stoichiometry identical to that obtained from a 1:1 ethanol-to-water mixture.

The DSMC method and the details of the numerical simulations, including the

gas phase and surface chemistry models, are described in §II. This is followed by a presentation of the numerical results for a range of operating conditions in §III. In §IV, the DSMC results are analyzed and compared to analytic expressions describing the behavior of the system in the low- and high-pressure limits. Details of the derivations of the analytic forms are given in the Appendix. Finally, the implications of our findings for diamond CVD are discussed and summarized in §V.

II. NUMERICAL MODEL

In this section we give a brief overview of the direct simulation Monte Carlo (DSMC) method. For a more comprehensive treatment, see Bird [3]. This is followed by a description of the one-dimensional computational domain, the gas-phase collision model, and the surface chemistry mechanism.

A. DSMC method

The degree of rarefaction of a gas flow is usually measured by the Knudsen number, $Kn \equiv \lambda/L$, where λ is the mean free path of the gas molecules and L is the smallest characteristic dimension of the system. The traditional Navier-Stokes treatment of gas dynamics breaks down at approximately $Kn = 0.1$, and must be replaced by an appropriate molecular model. Although molecular dynamics (MD) is valid in this regime, its implementation would be prohibitively expensive. An alternative approach is the DSMC method developed by Bird. DSMC is a particle method in which the molecular motion is modeled deterministically, while the binary collisions between molecules are treated statistically. Although DSMC has not been strictly proven to be equivalent to solving the Boltzmann equation, the technique is based on the dilute gas and molecular chaos assumptions used in its derivation. The DSMC method has been used primarily by the aerospace community in the study of rarefied flows [3],

but more recently has been applied to the modeling of CVD processes [12–15]. The applicability of the method is not limited to rarefied flows, but because the computational expense of the method increases proportionally to the density of the system, it is not generally used in flow regimes where the Navier-Stokes equations are valid. We will demonstrate quantitative agreement between our DSMC simulations and analytic results in the low- and high-pressure limits.

There are two key factors which make DSMC applicable to much larger systems than those tractable by MD. First, each simulated particle can represent an extremely large number of gas molecules. In the calculations performed in the present study, the ratio of real molecules to simulated molecules ranged from 5.72×10^{14} to 2.93×10^{17}. Second, a basic assumption in DSMC is that the convective motion of the particles can be decoupled from the intermolecular collisions on a timescale comparable to the mean collision time. This results in a much longer allowable timestep than in MD where the timestep is determined by the intermolecular force. The DSMC code used in this study is based on source code available from Bird, with modifications made for the surface reactions described below.

B. Gas-phase model

The model system used in the calculations consists of a gas mixture of either H/H_2 or $H/H_2/CO$ confined in one-dimension between a diamond growth surface at $x = 0$ and a hot activating surface at $x = L$ as shown in Fig. 1. The computational domain is divided into 100 equally spaced cells. The growth surface is maintained at a temperature of 1200 K for all cases and the activating surface is set to a temperature in the range 2000-4000 K. The interactions between the gas-phase species are treated using the variable soft sphere collision model [16, 17], which properly accounts for variations in the viscosities and self-diffusion constants of the gas-phase species as a

function of temperature. Rotational degrees of freedom for H_2 and CO are considered to be fully equilibrated at the local gas temperature. A discrete level model for the vibrational state of H_2 was included, but its effect was negligible since H_2 was found to be at most 15% vibrationally excited in the hottest region of the reactor. Equilibration between the translational, rotational, and vibrational degrees of freedom followed the Larsen-Borgnakke model [18]. The homogeneous (gas-phase) recombination of hydrogen atoms was originally considered, but was found to be negligible compared to the rate of recombination on the diamond surface. The parameters for the gas-phase species are listed in Table 1.

C. Surface model

The accommodation factor for all surface scattering processes is set to be unity, *i.e.*, incident molecules become completely thermally equilibrated with the surface and are reflected with translational, rotational, and vibrational energies chosen from the appropriate Boltzmann distribution. While this assumption is usually valid for heavy molecules, light species such as H and H_2 generally have accommodation coefficients less than unity because of the large mass differences between the incident molecules and the surface atoms. A large majority of the diamond surface sites are hydrogen terminated, however. Thus, most molecules incident on the surface will end up striking a hydrogen atom rather than a carbon atom, resulting in more complete accommodation. All gas-surface collisions other than atomic hydrogen scattering from the diamond growth surface and molecular hydrogen scattering from the activating surface are taken to be non-reactive.

The growth surface consists of two types of sites: hydrogen-terminated carbon sites and surface radical sites, denoted by C_dH and C_d^*, respectively. The corresponding fractional coverages of the growth surface by the two types of sites are given

by f^{H} and f^{*}. Two elementary gas-surface reactions involving hydrogen atoms are considered: the abstraction reaction

$$\mathrm{C}_d\mathrm{H} + \mathrm{H} \rightarrow \mathrm{C}_d^{*} + \mathrm{H}_2, \tag{1}$$

and the termination reaction [20]

$$\mathrm{C}_d^{*} + \mathrm{H} \rightarrow \mathrm{C}_d\mathrm{H}. \tag{2}$$

The first of these is responsible for the creation of surface radical sites where carbon addition can occur, while the second has the effect of passivating the growth surface. Taken together, these two reactions comprise the primary mechanism responsible for the conversion of atomic to molecular hydrogen under CVD conditions. The reverse processes of the above reactions are neglected. Goodwin [6] has estimated on the basis of thermochemistry that the equilibrium constant, k_f/k_r, for the abstraction reaction is approximately 800, while Coltrin and Dandy [21] propose a surface reaction probability of $\sim 4 \times 10^{-4}$ for the reverse process. The thermal desorption of hydrogen can be neglected on the basis of the large activation-energy barrier ($\sim$75 kcal/mol [22]) for the process.

Because of their key importance in diamond growth, the rates of these reactions have been of considerable interest. Since we are employing a particle-based simulation technique, it is convenient to express the gas-surface rate constants in terms of the surface reaction probabilities γ_{abs} and γ_{term}. The reaction probability can be related to the more familiar mass-action kinetic rate constant through

$$k_{f_i} = \left(\frac{\gamma_i}{1-\gamma_i/2}\right)\frac{1}{\Gamma^m}\left(\frac{RT}{2\pi W}\right)^{1/2}, \tag{3}$$

where Γ is the surface-site concentration (3.14×10^{15} sites cm^{-2} for diamond), m is the sum of the stoichiometric coefficients of the surface-phase reactants, and W is the molecular weight of the gas-phase species. The fractional coverages of the

surface can be expressed in terms of the reaction probabilities through the expressions $f^{\mathrm{H}} = \gamma_{term}/(\gamma_{term}+\gamma_{abs})$ and $f^{*} = \gamma_{abs}/(\gamma_{term}+\gamma_{abs})$. The probabilities of an incident gas-phase hydrogen atom abstracting a surface hydrogen or terminating a surface radical are equal and given by $\gamma_{term}\gamma_{abs}/(\gamma_{term}+\gamma_{abs})$.

Experimentally measured rates are not available for the surface reactions, and so estimates from analogous gas-phase reactions or numerical simulations must be used. The results presented in this paper were obtained using the values of $\gamma_{abs} = 0.04$ and $\gamma_{term} = 0.43$ (at 1200 K) proposed by Brenner *et al.* [23], based on molecular dynamics simulations employing empirical carbon-hydrogen potentials [24]. Other estimates for the surface reaction probabilities include $\gamma_{abs} = 0.22$, $\gamma_{term} = 1$ (Harris [25]), $\gamma_{abs} = 0.016$, $\gamma_{term} = 0.19$ (Harris and Belton [26]), and $\gamma_{abs} = 0.0037$, $\gamma_{term} = 0.016$ (Frenklach and Wang [27]). The parameters from the molecular dynamics simulations were chosen because, as pointed out by Goodwin [6], they account for the important physical effects of both energy transfer to the lattice and steric hindrance.

Although the rates of these elementary reactions have not been determined experimentally, related quantities have been measured. Harris and Weiner [28] cite a value of 0.12, with a level of accuracy of about a factor of two, for the probability of hydrogen atom recombination on the surface. It is important to distinguish between γ_{abs} and γ_{rec}. The former is the probability that a hydrogen atom striking a hydrogen-terminated surface site participates in an abstraction reaction, while the later is the likelihood that an incident hydrogen atom eventually reacts to form H_2 rather than scatter non-reactively. This quantity can be expressed in terms of the elementary reaction probabilities as

$$\gamma_{rec} = 2\gamma_{term}\gamma_{abs}/(\gamma_{term}+\gamma_{abs}). \tag{4}$$

Using high-resolution electron energy loss spectroscopy (HREELS), Thoms *et al.* [5]

were able to determine a value of 0.05 $\pm$ 0.01 for the ratio $\gamma_{abs}/\gamma_{term}$. The elementary reaction probabilities of Brenner *et al.* are reasonably consistent with both of these experimental studies.

The diamond surface chemistry described above results in the conversion of atomic to molecular hydrogen. For diamond growth to occur, a constant flux of hydrogen atoms to the growth surface is required. To provide a source of atomic hydrogen, H_2 molecules incident on the activating surface are allowed to dissociate with a probability γ_{diss}. Most of the results presented in this paper were obtained with γ_{diss} set equal to unity. The degree of hydrogen dissociation under CVD conditions is not always known and this choice for γ_{diss} allows us to establish an upper limit on the H atom flux for a given set of operating conditions.

III. NUMERICAL RESULTS

In this section, we present the results of our DSMC calculations. Since the parameter space of interest is too large to study completely, we have chosen a set of parameter values as standard conditions and looked at the effect of varying one parameter at a time from this set. Our standard conditions comprise a gas mixture of molecular and atomic hydrogen with L = 1 cm, T_{sub} = 1200 K, T_{act} = 3000 K, γ_{term} = 0.43, γ_{abs} = 0.04, and γ_{diss} = 1.0. The effect of varying each parameter was investigated over a range of reactor pressures P. This allows us to compare the numerical results to the analytic expressions in both the low- and high-pressure limits. We can also determine the range of validity of the analytic forms and obtain quantitative results in the transition regime.

In all of the calculations, the system is initialized with a linear temperature gradient extending across the length of the computational domain. The gas-phase composition is initially uniform everywhere with atomic and molecular hydrogen mole

fractions of 2/3 and 1/3, respectively. The temperature and species gradients are allowed to evolve until the steady-state conditions are reached. Statistics are collected over 20,000-80,000 DSMC timesteps only after it is clear that the temperature and concentration gradients are no longer evolving. The pressure of the system is not set since we cannot predict *a priori* the total number of particles in the final state. Instead, we set the initial gas density and determine the pressure at the end of the calculation by evaluating the net momentum transfer to the bounding surfaces. In all cases, the pressures measured at the two walls agreed to within less than 0.1%. The difference between the heat fluxes at the substrate and activating surface ranged from 0.1% at low pressures to at most 1% at high pressures.

The main focus of this work is the effect of the reactor operating conditions on the hydrogen atom flux (ϕ_{H}) to the growth surface. Also of interest is the partitioning of the total heat flux (q_{tot}) to the substrate into contributions due to thermal conduction (q_{cond}) and hydrogen atom recombination (q_{rec}). The recombinative heat flux is related to the H-atom flux through the expression

$$q_{rec} = \phi_{\mathrm{H}} \gamma_{rec} \Delta H^f / 2, \tag{5}$$

where $\Delta H^f = 104.2$ kcal mol^{-1} is the heat of formation of atomic hydrogen from molecular hydrogen. The conductive heat flux q_{cond} is defined as the difference between the total (kinetic + rotational + vibrational) energies of the incident and reflected molecules. The energy flux due to the conversion of two hydrogen atoms with six degrees of freedom into a single hydrogen molecule with five degrees of freedom is accounted for by q_{cond}.

A. Effect of separation between substrate and heat source

In Fig. 2, the species and temperature profiles for an H/H_2 mixture at pressures of 0.050, 0.45, and 6.6 Torr are shown. At low pressures, rarefied gas effects are clearly

observed. Most notably, the temperature profile does not vary continuously from 1200 K to 3000 K as predicted from continuum theory, but exhibits jump discontinuities at the surfaces typical of high Kn flows. The temperature jump is a direct consequence of the extremely low density of the gas, since individual gas molecules travel relatively large distances before undergoing thermalizing collisions. As the pressure is increased, the continuum regime is approached and the temperature jump is diminished. The effect of pressure on the species profiles is also quite profound. At 0.050 Torr, the hydrogen is almost completely dissociated and there is little spatial variation in the gas phase composition. As the pressure is increased, the counter-diffusion of the two species is retarded and larger concentration gradients develop.

The hydrogen-atom flux, total heat flux, and the contributions from thermal conduction and hydrogen recombination are shown in Fig. 3 as a function of pressure for values of L equal to 0.25, 0.5, and 1.0 cm. In the low-pressure limit, q_{cond} and q_{rec} exhibit a linear dependence on pressure and are independent of L. At higher pressures, the components of the heat flux asymptote to constant values that are strongly dependent on L. At a pressure in the range of 0.5-2.0 Torr, a crossover between q_{cond} and q_{rec} occurs. In the low-pressure limit, q_{cond} is greater than q_{rec}, while at 25 Torr, q_{rec} exceeds q_{cond} by a factor of 2-4.

B. Effect of CO dilution

In Fig. 4, the species and temperature profiles for the $H/H_2/CO$ mixture with a CO-H stoichiometry of 1:4 are shown for three different pressures. The temperature and hydrogen profiles show the same trends as were seen in the H/H_2 mixture, but small quantitative differences exist between the temperature profiles. A comparison of Figs. 2a and 4a shows that the temperature jump at the walls is slightly less for the $H/H_2/CO$ mixture. This is due to the fact that the addition of carbon monoxide

to the gas phase reduces the average molecular mean-free path. The influence of thermal diffusion (Soret effect), the preferential diffusion of lighter species toward regions of higher temperature, can be seen in the CO profiles. The CO mole fraction for the simulation carried out at 6.5 Torr, *e.g.*, varies from 0.3 at the substrate to 0.2 at the activating surface. Additional calculations were performed in which the mass of CO was reduced to that of atomic hydrogen, or the surface reactions were turned off to eliminate the counter-flows of H and H_2. The results confirm that the CO concentration gradient is due to thermal diffusion driven by the disparate masses of CO and H/H_2.

The hydrogen atom and thermal fluxes are shown in Fig. 5 for the $H/H_2/CO$ mixture. Also displayed for comparison are the results for the H/H_2 mixture. The general trends and behavior of q_{tot}, q_{rec}, and q_{cond} are the same for the two cases, with both q_{cond} and q_{rec} consistently lower for the $H/H_2/CO$ mixture. Although CO comprises only about 25% of the gas mixture by mole fraction, the effects on the fluxes are much larger. The high-pressure limit of q_{cond} is reduced by roughly a factor of two. The recombinative heat flux has not yet reached its asymptotic value, but it appears to be reduced by a factor in the range 1.5–2. Because of its large mass and size, as compared to atomic and molecular hydrogen, the carbon monoxide significantly retards the counter-diffusion of the hydrogen species. This leads to a severe reduction of both q_{cond} and q_{rec}.

C. Effect of temperature at activating surface

A series of calculations were carried out to determine the effect of variations in the temperature at the activating surface on the hydrogen-atom and heat fluxes. The results are shown in Fig. 6 for the H/H_2 mixture with $L = 1$ cm. As expected from continuum theory assuming a $T^{2/3}$ dependence of the thermal conductivity, the

conductive heat flux in the high-pressure limit is roughly proportional to $(T_{act}^{5/3} - T_{sub}^{5/3})$. At high pressures, q_{cond} rises steadily but more slowly with T_{act}. q_{rec} likewise increases monotonically with T_{act} at high pressures, but the changes are relatively small. Over the temperature range $2000 \leq T_{act} \leq 4000$, q_{rec} varies by only about 25%. In contrast, at low pressures q_{rec} shows the counterintuitive behavior of decreasing as T_{act} is increased. This is due to the fact that the increased thermal velocities of the molecules are more than offset by the lower gas density as will be shown in the next section. For our choice of operating conditions, the dependence of q_{rec} on T_{act} crosses over from the low- to high-pressure behaviors for pressures in the range of a few Torr.

D. Effect of H_2 dissociation probability

All of the results presented to this point were obtained assuming a 100% dissociation of molecular hydrogen at the activating surface. The various activation techniques used in CVD reactors can lead to the direct dissociation of H_2 through mechanisms other than neutral gas-phase chemistry - *e.g.*, electron impact dissociation in a plasma - resulting in elevated H/H_2 ratios. Nonetheless, 100% dissociation of H_2 is clearly an optimal upper bound. In this section we consider the effect of incomplete dissociation of H_2 at the activating surface. Figure 7 compares the results for H_2-H mixtures with L equal to 1 cm for γ_{diss} set to 1.0, 0.5, and 0.1.

The conductive component of the heat flux is very insensitive to the value of γ_{diss}. Reducing γ_{diss} from 1.0 to 0.5 results in negligible changes in q_{cond}, while further decreasing γ_{diss} to 0.1 leads to at most a few percent reduction in q_{cond}. A detailed explanation for this behavior will be given in §IV, but it can be at least be partially understood in terms of the species profiles for the $\gamma_{diss} = 1.0$ and 0.1 cases shown in Fig. 8. In the low-pressure limit, the degree of hydrogen dissociation depends strongly on γ_{diss}. Because the molar heat fluxes for atomic and molecular

hydrogen in the free-streaming limit differ by less than 20%, the effect on the thermal conductivity of the mixture is relatively small. At high pressures, the composition and hence the thermal conductivity of the gas depends only weakly on γ_{diss}. Although q_{rec} shows a stronger dependence on γ_{diss} than does q_{cond}, the variation of q_{rec} with γ_{diss} is still rather small until γ_{diss} is reduced to 0.1.

E. Effect of surface reaction probabilities

It was pointed out in §IIc that there is considerable uncertainty in the probabilities of the gas-surface reactions. None of the reaction rates are at present available experimentally, so the rates must be either derived from first principles or taken from analogous gas phase reactions. While the values for γ_{abs} and γ_{term} proposed by various investigators vary by almost two orders of magnitude, the ratio $\gamma_{term}/\gamma_{abs}$ lies within a much narrower range. The values proposed by Brenner *et al.* are consistent with the hydrogen recombination probability γ_{rec} measured by Harris and Weiner [28], but this agreement does not guarantee the validity of their values.

In Fig. 9, we compare the results of simulations on the H/H_2 mixture for three different sets of surface reaction probabilities. In the first case, our standard values from Brenner *et al.* [23, 24] ($\gamma_{term} = 0.43$ and $\gamma_{abs} = 0.04$) are used. In the second case, the probabilities of both surface reactions are doubled. Since the fractions of the surface sites in the two types of configurations, C_dH and C_d^*, are determined solely by the ratio $\gamma_{term}/\gamma_{abs}$, changing the surface reaction probabilities in this way has no effect on the state of the surface. Finally, in the third case, γ_{abs} is doubled while γ_{term} is left unchanged.

Variations in the surface reaction probabilities have virtually no effect on q_{cond}. The explanation for this behavior is identical to that given in the previous section. In the low-pressure limit, the heat flux depends very weakly on the degree of hydrogen

dissociation, while in the high-pressure limit, the gas-phase composition is nearly independent of the surface reaction probabilities. The quantities q_{rec} and $\phi_{\rm H}$ depend strongly on γ_{abs}, but are nearly independent of the value for γ_{term}. This is because the total recombination probability, $\gamma_{rec} = 2\gamma_{abs}\gamma_{term}/(\gamma_{abs} + \gamma_{term})$, is approximately $2\gamma_{abs}$ so long as $\gamma_{term} \gg \gamma_{abs}$. At high pressures, the recombinative heat fluxes for the three cases appear to be converging, while at low pressures the hydrogen atom flux is independent of γ_{abs}.

IV. ANALYSIS

Our model system can be analyzed to derive expressions for the particle and energy fluxes in both the low- and high-pressure regimes. In this section, these results are presented and then used to interpret and understand further the DSMC simulations described above. Details of the derivations are relegated to the Appendix.

A. Low-pressure regime

At low pressures, the gas can be treated as a mixture of counter-streaming populations which collide only with the bounding surfaces. Requiring the oppositely directed mass fluxes to balance at those surfaces fixes the relative populations of cold and hot particles of each species separately and those of H atoms and H_2 molecules jointly. The results are

$$\phi_{\rm H} = n\left(2k_B/\pi m_{\rm H}\right)^{1/2} \frac{T_{act}^{1/2}T_{sub}^{1/2}}{\left(1-\gamma_{rec}\right)T_{act}^{1/2} + T_{sub}^{1/2}} X_{\rm H}, \tag{6}$$

$$P = nk_B T_{act}^{1/2}T_{sub}^{1/2}\left[\frac{T_{act}^{1/2} + \left(1-\gamma_{rec}\right)T_{sub}^{1/2}}{\left(1-\gamma_{rec}\right)T_{act}^{1/2} + T_{sub}^{1/2}} X_{\rm H} + \frac{\left(1-\gamma_{diss}\right)T_{act}^{1/2} + T_{sub}^{1/2}}{T_{act}^{1/2} + \left(1-\gamma_{diss}\right)T_{sub}^{1/2}} X_{\rm H_2} + X_{\rm CO}\right], \tag{7}$$

$$q_{cond} = \left(2/\pi\right)^{1/2} nk_B^{3/2} T_{act}^{1/2}T_{sub}^{1/2}\left(T_{act}^{1/2} - T_{sub}^{1/2}\right)$$

$$\times \left(2m_{\rm H}^{-1/2} X_{\rm H} + 3m_{\rm H_2}^{-1/2} X_{\rm H_2} + 3m_{\rm CO}^{-1/2} X_{\rm CO}\right)$$
$$+ \phi_{\rm H} \gamma_{rec} k_B \left(T_{act} - T_{act}^{1/2} T_{sub}^{1/2} + T_{sub}\right)/2, \tag{8}$$

$$q_{rec} = \phi_{\rm H} \gamma_{rec} k_B T_{bind}/2, \tag{9}$$

and

$$\frac{\gamma_{rec}}{(1-\gamma_{rec})\,T_{act}^{1/2} + T_{sub}^{1/2}}\, X_{\rm H} = 2^{1/2} \frac{\gamma_{diss}}{T_{act}^{1/2} + (1-\gamma_{diss})\,T_{sub}^{1/2}}\, X_{\rm H_2}. \tag{10}$$

In these equations, m_s and X_s are the mass and fractional concentration, respectively, of species s, and $T_{bind} = \Delta H^f/k_B = 5.25 \times 10^4$ K is the binding energy of the H_2 molecule expressed as a temperature. The contributions of H_2 and CO to the conductive heat flux in (8) are enhanced over that of H by a factor of 3/2, due to excitation of the two rotational degrees of freedom of the diatomic molecules. Excitation of the vibrational degrees of freedom of H_2 and CO was ignored in the analysis, in light of our DSMC results. The recombination and dissociation reactions contribute through the conversion at the substrate of two H atoms with six degrees of freedom into a single H_2 molecule with five degrees of freedom, and the inverse process at the activating surface. If these reactions do not occur, *i.e.*, $\gamma_{rec} = \gamma_{diss} = 0$, then the expressions above reduce to those given elsewhere [3], or to trivial identities.

The particle and energy fluxes and the pressure are all linear in the number density in the free-streaming regime. Consequently, if the temperatures and reaction probabilities are held fixed, the fluxes will scale linearly with the pressure. The fluxes also are predicted to be independent of the separation between the substrate and the activation source. Both of these trends are consistent with the low-pressure behavior of our DSMC simulations. A comparison between the lowest pressure H/H_2 DSMC simulations and the analytic forms is given in Table 2. The quantitative agreement between the two approaches is very good. It is worth noting that the discrepancy

in the value for q_{cond} is smallest for the largest Knudsen number case, $L = 0.25$ cm. As the separation between the substrate and the activating surface is increased, with pressure held fixed, collisional effects become more important and the free-streaming approximation loses validity. The effect of L on the transition from a collisionless to a collisional regime can also be seen in Fig. 3b. As L is decreased, the fluxes exhibit linear scaling over a larger pressure range.

The large dissociation fraction in our standard case is due to the high probability of H_2 dissociation at the activating wall relative to that of H atom recombination at the substrate. Rearranging Eq. (10) yields

$$X_{H_2} = 2^{-1/2} \frac{\gamma_{rec}}{\gamma_{diss}} \frac{T_{act}^{1/2} + (1 - \gamma_{diss}) T_{sub}^{1/2}}{(1 - \gamma_{rec}) T_{act}^{1/2} + T_{sub}^{1/2}} X_H. \tag{11}$$

Thus, $\gamma_{rec} \ll \gamma_{diss} \leq 1$ implies $X_{H_2} \ll X_H$, and quite generally the relative concentrations are very sensitive to the relative surface reaction probabilities. We observed these trends in our calculations with variable reaction rates, particularly those shown in Fig. 8. At the same time, we found the conductive heat fluxes in Figs. 7 and 9 to be essentially independent of the H/H_2 ratio. This is because the thermal conductivities of H and H_2, as inferred from Eq. (8), are nearly identical: the larger mass of the molecule is compensated by its extra, rotational degrees of freedom. The recombinative heat flux, in contrast, shows two distinct trends. As shown in Fig. 7, it is sensitive to the dissociation probability γ_{diss} only when the latter is very small. This follows immediately from Eq. (11), since for $\gamma_{diss} \approx \gamma_{rec}$, the H_2 and H concentrations become comparable. The resulting drop in X_H produces a proportional decline in the hydrogen-atom and recombinative heat fluxes. So long as $\gamma_{rec} \ll \gamma_{diss}$, the hydrogen concentration is insensitive to these probabilities. The recombinative heat flux, however, is directly proportional to γ_{rec}, as indicated by Eq. (9) and illustrated in Fig. 9. Both of these trends just reflect the fact that the slow recombination of H atoms at

the substrate is a rate-limiting step in this process.

We noted in Fig. 6 that varying the temperature of the activating surface has a pronounced effect on the conductive heat flux but a very limited impact on the hydrogen atom and recombinative heat fluxes. As a first approximation, we can reduce Eqs. (7) and (8) to $P = nk_B T_{act}^{1/2} T_{sub}^{1/2}$ and $q_{cond} = (8/\pi)^{1/2} n k_B^{3/2} T_{act}^{1/2} T_{sub}^{1/2} (T_{act}^{1/2} - T_{sub}^{1/2})$, respectively. This leads to the result

$$q_{cond} \propto P(T_{act}^{1/2} - T_{sub}^{1/2}). \tag{12}$$

Using this expression we find that the ratio $q_{cond}(T_{act} = 4000)/q_{cond}(T_{act} = 2000)$ is equal to 2.8, in excellent agreement with the lowest pressure numerical results which yield a ratio of 2.7. Retaining the terms that have been omitted in the derivation of Eq. (12) further improves the agreement between the two sets of results. These smaller terms are important in the calculation of the recombinative heat flux, whose temperature dependence is more subtle and requires a more careful derivation. Using Eqs. (6), (7), (9), and (10) we find

$$q_{rec}, \phi_{\mathrm{H}} \propto \frac{P}{T_{act}^{1/2} + (1 - \gamma_{term}) T_{sub}^{1/2} + (\gamma_{term}/2^{1/2}\gamma_{diss})[(1 - \gamma_{diss}) T_{act}^{1/2} + T_{sub}^{1/2}]} \tag{13}$$

Although the effect is relatively small, increasing T_{act} for fixed pressure leads to a decrease in q_{rec}, as shown in Fig. 6b. The increase in the average thermal speed with increasing T_{act} in Eq. (6) is more than offset by the simultaneous reduction in the total number density.

Under our standard conditions it happens that the conductive heat flux is greater than the recombinative component. Making the reasonable approximations $\gamma_{rec} \ll 1$, $X_{\mathrm{H}_2} \ll X_{\mathrm{H}}$, and $T_{bind} \gg T_{act}$, we find from Eqs. (8) and (9) that

$$\frac{q_{cond}}{q_{rec}} \approx \frac{T_{act} - T_{sub}}{\gamma_{rec} T_{bind}/4}. \tag{14}$$

Thus, as is illustrated in Figs. 6 and 9, the flux ratio is sensitive to the temperature of the activating surface (through its effect on the magnitude of the conductive flux) and to the recombination probability of H atoms at the substrate (which affects the size of the recombinative flux).

Finally, adding carbon monoxide as a diluent at low pressures has the principal effect of reducing both the atomic and molecular hydrogen concentrations proportionately, and therefore the H atom flux and the heat fluxes. CO contributes to the conductive flux much more weakly due to its larger mass (and consequently longer transit time between the activating surface and substrate). Thus, a reduction in the heat fluxes of between 12.5% and 25% – depending upon the extent to which H_2 is dissociated in the gas – is expected. The observed effects in Fig. 5 are somewhat larger than this, evidently due to the effects of rare but not inconsequential collisions with CO molecules. We noted the latter in conjunction with the temperature profiles of Fig. 4.

B. High-pressure regime

At high pressures, the gas can be analyzed using a hydrodynamical description. This generally involves the solution of a set of coupled, highly nonlinear partial differential equations. As detailed in the Appendix, a few simplifying assumptions permit us to draw some analytically tractable conclusions which turn out to be quantitatively useful. The approximate results for a pure H/H_2 mixture are

$$\phi_{\mathrm{H}} \approx \ln 2 \left(d^{act}_{\mathrm{H-H_2}} + d^{sub}_{\mathrm{H-H_2}} \right) / \gamma_{rec} L, \tag{15}$$

$$q_{cond} \approx \left(\kappa^{act}_{\mathrm{H}} + \kappa^{sub}_{\mathrm{H_2}} \right) (T_{act} - T_{sub}) / 2L + 3 \phi_{\mathrm{H}} \gamma_{rec} k_B (T_{act} + T_{sub}) / 8, \tag{16}$$

$$q_{rec} = \phi_{\mathrm{H}} \gamma_{rec} k_B T_{bind} / 2, \tag{17}$$

and

$$\gamma_{rec} T_{sub}^{-1/2} X_{\rm H}^{sub} = 2^{1/2} \gamma_{diss} T_{act}^{-1/2} X_{\rm H_2}^{act}$$
$$\approx (2\pi m_{\rm H} k_B)^{1/2} \ln 2 \left(d_{\rm H-H_2}^{act} + d_{\rm H-H_2}^{sub} \right) / PL. \qquad (18)$$

In these equations, $d_{\rm H-H_2} \equiv n D_{\rm H-H_2}$, where $D_{\rm H-H_2}$ is the coefficient for binary diffusion of H atoms through H_2 molecules, and $\kappa_{\rm H}$ and $\kappa_{\rm H_2}$ are the thermal conductivities of atomic and molecular hydrogen. All of these transport coefficients vary with temperature, which has been taken into account in an approximate way by simply averaging the values at the substrate and activating surface. For our standard case, the average diffusion constant and thermal conductivity are 2.0×10^{20} cm^{-1} s^{-1} and 1.2×10^{-2} W cm^{-1} K^{-1}, respectively.

The fluxes (15)–(17) are independent of pressure, indicating that a saturation of the fluxes occurs as the pressure increases from the free-streaming regime. They also depend inversely on the separation L between the substrate and activating surface, the only macroscopic scale length in our system. These are very general features of the hydrodynamic description, independent of any other simplifying approximations that have been made to derive the above expressions. The two behaviors are exhibited by our DSMC results in the high-pressure limit, particularly those for the conductive heat fluxes. The hydrogen-atom and recombinative heat fluxes have not quite saturated at the maximum pressures assumed in the DSMC runs, but the trend in this direction is fairly clear. Quantitatively, we compare results from our highest-pressure DSMC simulations with the analytic forms in Table 3. Given the approximations inherent in our analysis, the agreement with the DSMC values is very good. As is to be expected, the closest correspondence is obtained for the largest gap, and thus the most collisional system, $L = 1$ cm.

All of the fluxes depend implicitly on the temperature of the activating surface

through the transport coefficients for thermal conduction and binary diffusion. These coefficients rise monotonically over the temperature range of interest. Thus, as is evident in Fig. 6, the atomic hydrogen and recombinative heat fluxes increase as the activating surface temperature increases. The numerical values rise by about 25% as T_{act} varies from 2000 to 4000 K. From the atomic data, an increase of about 40% in the diffusion coefficient, and thus the fluxes, is expected. This discrepancy probably just reflects the clearly incomplete convergence of the DSMC fluxes to their asymptotic values. The conductive heat fluxes, which have more nearly converged, increase due to both the greater temperature difference between substrate and activating surface and the enhanced conductivity. Here, we can analytically estimate 8.2 and 40.0 W cm^{-2} for $q_{cond}(T_{act} = 2000K)$ and $q_{cond}(T_{act} = 4000K)$, respectively, in quite good agreement with the values in Fig. 6.

The analysis predicts that the heat and H-atom fluxes are independent of the dissociation probability for H_2 molecules at the activating surface. As seen in Fig. 7, this is true to a high degree of accuracy for the conductive heat fluxes and is true of the H-atom and recombinative heat fluxes except at very low dissociation probability, $\gamma_{diss} = 0.1$. Careful inspection of the figure suggests, however, that all of the curves for these fluxes are indeed converging as the pressure increases. Indeed, it appears that the divergence of the curves just reflects a slower approach to the asymptotic fluxes when γ_{diss} is small. Specifically, we note from (18) that the H_2 concentration at the activating surface declines to its asymptotic value of zero as $(\gamma_{diss}P)^{-1}$. Thus, the convergence with increasing pressure of the species profiles, and consequently the particle fluxes, is slower for smaller values of the dissociation probability. The same statement is true with respect to the recombination probability of H atoms at the substrate. Evidently, it is in fact the very small value of γ_{rec} (= 0.073) that delays the convergence of the species profiles and the saturation of the fluxes in all of the

cases we have examined. As corroboration for this assertion we refer to the species profiles in Fig. 8, which show that the H concentration at the substrate is still about 20% at 24 Torr of pressure, while the H_2 concentration at the activating surface is nearly zero.

Varying the recombination probability γ_{rec} has an effect on the heat fluxes similar to that of varying γ_{diss}: doubling γ_{rec} has no discernible effect on the conductive heat fluxes, and seems only to hasten the saturation of the recombinative flux as the pressure increases, without changing its asymptotic value. The H-atom flux to the substrate, on the other hand, is reduced by a factor of two (see Fig. 9). This result is in accord with the analytical result (15), wherein ϕ_H is inversely proportional to γ_{rec}. Physically, this happens because the rate at which H atoms can be transported to the substrate is limited by the binary diffusion coefficient; increasing the recombination probability simply reduces the (asymptotically small) concentration of H atoms at the substrate until the recombination and diffusion rates come into balance. It is interesting to note that the effect of γ_{rec} at high pressures is the opposite of that at low pressures, where it had no effect on the H-atom flux but contributed proportionately to the associated recombinative flux. This is reflected also in the ratio of the conductive and recombinative heat fluxes,

$$\frac{q_{cond}}{q_{rec}} \approx \frac{\kappa_H^{act} + \kappa_{H_2}^{sub}}{d_{H-H_2}^{act} + d_{H-H_2}^{sub}} \frac{T_{act} - T_{sub}}{\ln 4 \; k_B T_{bind}}, \tag{19}$$

whose independence of γ_{rec} contrasts sharply with the flux ratio (14) at low pressures.

V. SUMMARY AND CONCLUSIONS

One-dimensional DSMC calculations have been carried out for the purpose of studying diffusion-dominated diamond CVD processes. The effects of pressure, distance between the substrate and the activating surface, gas-phase composition, reactor temperature, surface reaction probabilities, and degree of molecular hydrogen

dissociation on the hydrogen-atom and thermal fluxes to the diamond surface were investigated. To supplement and aid in the interpretation of the numerical results, analytic expressions were derived for the low- and high-pressure limits. Good quantitative and qualitative agreement was found between the two approaches.

Several of the model parameters were shown to play a critical role in determining the heat and hydrogen-atom fluxes to the surface. In many instances, the effect of varying a particular parameter depends sensitively upon the pressure regime in which one operates. At low pressures, the H-atom and heat fluxes all scale directly with the gas pressure, *i.e.*, the number density of particles. The greater the number of carriers (of mass, momentum, or energy), the larger the fluxes that can be supported by streaming of particles between the activating surface and the substrate. At high pressures, in contrast, the fluxes eventually saturate at fixed values. In this collisional regime, increasing the number of carriers by raising the pressure is exactly compensated for by the concomitant increase in the density of scatterers, which impedes the transport of mass, momentum, and energy across the gap.

A reciprocal role is played by the distance separating the activating surface and the substrate. The particles free-stream between the two at very low pressures, so the fluxes are independent of the separation. At high pressures, on the other hand, the fluxes are driven by the gradients in the temperature and composition across the gap. The strength of these gradients and their associated thermodynamic forces vary inversely as the width of the gap.

We examined the effect of oxygen-bearing species in diamond CVD by adding carbon monoxide to the hydrogen mixture. CO reduces all of the fluxes to the substrate and activating surface. In the low-pressure limit, the total fluxes are just a linear superposition of independent contributions from each species. As a result, the H and H_2 fluxes are diminished exactly in proportion to the CO mole fraction. At higher

pressures, CO has the further effect of substantially retarding the counter-diffusion of atomic and molecular hydrogen through collisions with those species. Thus, the detrimental influence of CO addition on the H-atom transport rises as the pressure increases.

Varying the temperature of the activating surface produced only subtle effects on the hydrogen-atom and recombinative heat fluxes. At low pressures, these fluxes exhibit the counter-intuitive behavior of decreasing as the temperature T_{act} increases at fixed pressure. This is due to the decline in the number density of the gas as the average temperature is raised. A cross-over occurs at intermediate pressures, to the high-pressure behavior of the fluxes rising slowly with rising T_{act}. The increased efficacy of diffusion of H through H_2 at higher temperatures is responsible for this (weak) trend.

As one would expect, in contrast the activating temperature has a very strong influence on the conductive heat flux. q_{cond} increases monotonically with increasing T_{act}, from the rather slow dependence as $(T_{act}^{1/2} - T_{sub}^{1/2})$ in the free-streaming regime at low pressures, to the much steeper dependence as roughly $(T_{act}^{5/3} - T_{sub}^{5/3})$ in the continuum regime at high pressures. The latter reflects an approximate $T^{2/3}$ dependence of the thermal conductivity of the gas on its temperature.

In addition to the operating parameters which can be varied and monitored in an experimental CVD reactor, we also have studied the role of the surface reaction and dissociation rates. The probabilities of H-atoms terminating a reactive site, γ_{term}, and abstracting another H atom from a previously terminated site to form H_2, γ_{abs}, jointly determine both the state of the surface and the total probability of H-atom recombination on the surface, $\gamma_{rec} = 2\gamma_{abs}\gamma_{term}/(\gamma_{abs} + \gamma_{term})$. Although the absolute values of these reaction probabilities are quite uncertain, there is a consensus that the termination reaction is much faster than the abstraction reaction, $\gamma_{term} \gg \gamma_{abs}$.

This implies that the rate of the termination reaction has essentially no effect on the total recombination probability, since $\gamma_{rec} \approx 2\gamma_{abs}$, and therefore does not influence any of the particle or heat fluxes.

The rate of the abstraction reaction (and thus of hydrogen recombination at the diamond surface), on the other hand, has strong and complementary affects on the hydrogen-atom and recombinative heat fluxes in the low- and high-pressure regimes. At low pressures, the flux of H atoms is essentially independent of γ_{rec}; thus the recombinative heat flux (which is just proportional to $\gamma_{rec}\phi_{\mathrm{H}}$) increases linearly with the recombination probability. At high pressures, the rate of replenishment of hydrogen atoms at the substrate is limited by their rate of diffusion from the activating surface through the H_2 population. This (fixed) replenishment rate balances the loss rate $\gamma_{rec}\phi_{\mathrm{H}}$ of H atoms at the diamond surface. Thus, the total H-atom flux decreases inversely with the recombination probability; and the associated recombinative heat flux is then independent of γ_{rec}.

In contrast to these effects on ϕ_{H} and q_{rec}, the abstraction and recombination probabilities have a negligible impact on the conductive heat flux q_{cond}. At low pressures, the composition of the gas is sensitive to the relative rates of H-atom recombination and H_2-molecule dissociation, but the thermal conductivities of the two gases are very similar. At high pressures, the difference between the conductivities of the gases is greater, but the composition profiles are only weakly dependent upon the recombination probability. Thus, the conductive heat flux varies very little with γ_{rec} over the entire pressure range.

Finally, our standard conditions assume that the H_2 dissociation probability at the activating surface is unity. Generally, the gas composition and the particle and heat fluxes are essentially independent of the H_2 dissociation rate so long as it is much faster than the H recombination rate. When those two rates become comparable, the

H-atom and recombinative heat fluxes decline at low pressures due to the decrease in the H-atom concentration. These effects gradually fade at higher pressures, as the species profiles become independent of the reaction probabilities. The conductive heat flux is essentially unaffected by γ_{diss} at all pressures.

Our numerical model can be extended and improved to make it more applicable to real diamond CVD reactors. For example, in plasma-enhanced CVD (PECVD), molecular hydrogen dissociation and heating of the gas occurs through electron-stimulated reactions rather than interactions with an activating surface. Using the appropriate collision cross sections and electron densities, the surface heating and dissociation can be replaced by volumetric processes. In the present model, carbon addition to the diamond surface is ignored. Future work should treat the growth species as a perturbation on the pure H/H_2 mixtures, in which case diamond growth mechanisms also could be introduced into the model.

In conclusion, we have shown that the DSMC method can be used to both predict general trends and obtain quantitatively accurate results for the heat and hydrogen-atom fluxes to the surface in diffusion-dominated CVD diamond reactors. While excellent agreement was found between the numerical and analytical approaches in the low- and high-pressure limits, the DSMC technique has its greatest utility in the analytically intractable regime between these two regimes.

ACKNOWLEDGMENTS

The authors thank James E. Butler and Vasgen A. Shamamian for lending their expertise in diamond CVD. We also thank Graeme Bird, Elaine S. Oran, and Choong K. Oh for helpful suggestions regarding practical aspects of the DSMC simulations. Computations were carried out primarily on facilities at the Maui High-Performance Computing Center, under the auspices of the Department of Defense High Perfor-

mance Computing initiative. This work was supported by the Advanced Research Projects Agency.

REFERENCES

[1] F.G. Celli and J.E. Butler, Ann. Rev. Chem. **42**, 643 (1991).

[2] J.C. Angus, F.A. Buck, M. Sunkara, T.F. Groth, C.C. Hayman, and R. Gat, MRS Bull. **14**, 38 (1989).

[3] G.A. Bird, *Molecular Gas Dynamics and the Direct Simulation of Gas Flow* (Clarendon Press, Oxford, 1994).

[4] J.E. Butler and R.L. Woodin, Phil. Trans. R. Soc. Lond. A **342**, 209 (1993).

[5] B.D. Thoms, J.N. Russell, Jr., P.E. Pehrsson, and J.E. Butler, J. Chem. Phys. **100**, 8425 (1994).

[6] D.G. Goodwin, J. Appl. Phys. **74**, 6888 (1993).

[7] P.K. Bachmann, D. Leers, and H. Lydtin, Diamond Relat. Mater. **1**, 1 (1991).

[8] R.A. Rudder, G.C. Hudson, J.B. Posthill, R.E. Thomas, R.C. Hendry, D.P. Malta, R.J. Markunas, T.P. Humphreys, and R.J. Nemanich, J. Appl. Phys. **60**, 329 (1991)

[9] L. Kostadinov and D. Dobrev, Surf. Coat. Technol. **47**, 623 (1991).

[10] R.S. Sinkovits, C.R. DeVore, V.A. Shamamian, and C.K. Westbrook, Diamond Relat. Mat. **4**, 1277 (1995).

[11] R.S. Sinkovits, C.R. DeVore, and V.A. Shamamian, submitted to Diamond Relat. Mat. (1996).

[12] M. Ikegawa and J. Kobayashi, J. Electrochem. Soc. **136**, 2982 (1989).

[13] K. Nanbu, S. Igarashi, and S. Mitamura, Rep. Inst. Fluid Sci., Tohuku Univ. **3**, 35 (1991).

[14] D.G. Coronell and K.F. Jensen, J. Electrochem. Soc. **139**, 2264 (1992).

[15] D.G. Coronell and K.F. Jensen, J. Electrochem. Soc. **141**, 2545 (1994).

[16] K. Koura and H. Matsumoto, Phys. Fluids A **3**, 2459 (1991).

[17] K. Koura and H. Matsumoto, Phys. Fluids A **4**, 1083 (1992).

[18] C. Borgnakke and P.S. Larsen, J. Comput. Phys. **18**, 405 (1975).

[19] R.J. Kee, G. Dixon-Lewis, J. Warnatz, M.E. Coltrin, and J.A. Miller, "A Fortran computer code package for the evaluation of gas-phase multicomponent transport properties," Sandia National Laboratories Report, SAND86-8246 (1986).

[20] Reaction (2) is often referred to in the literature as the adsorption or recombination reaction. Throughout this paper we will be consistent in calling it the termination reaction.

[21] M.E. Coltrin and D.S. Dandy, J. Appl. Phys. **74**, 5803 (1993).

[22] D.D. Koleske, S.M. Gates, B.D. Thoms, J.N. Russell, Jr., and J.E. Butler, Surf. Sci. **320**, L105 (1994).

[23] D.W. Brenner, D,H, Robinson, R.J. Carty, D. Srivasta, and B.J. Garrision, in *Computational Methods in Materials Science*, edited by J.E. Mark, M.E. Glickman, and S.P. Marsh (Materials Research Society, Pittsburgh, PA 1992), pp. 255-260.

[24] D.W. Brenner, Phys. Rev. **B 42**, 9458 (1990).

[25] S.J. Harris, Appl. Phys. Lett. **56**, 2298 (1990).

[26] S.J. Harris and D.N. Belton, Thin Solid Films **212**, 193 (1992).

[27] M. Frenklach and H. Wang, Phys. Rev. B **43**, 1520 (1991).

[28] S.J. Harris and A.M. Weiner, J. Appl. Phys. **74**, 1022 (1993).

[29] R.B. Bird, W.E. Stewart, and E.N. Lightfoot, *Transport Phenomena* (Wiley, New York, 1960).

APPENDIX: DERIVATION OF ANALYTIC FORMS

1. Low-pressure regime

At low pressures, the counterstreaming populations of particles from the activating surface and the substrate are assumed to be thermalized distributions (*i.e.*, one-sided Maxwellians) at the temperatures T_{act} and T_{sub}, respectively. Denoting the scalar velocity component normal to the wall $v_\perp$ and the transverse vector component $\mathbf{v}_{||}$, the velocity distribution is

$$f\left(v_\perp, \mathbf{v}_{||}\right) = \begin{cases} 2n\left(2k_BT/\pi m\right)^{3/2}\ \mathrm{e}^{-m\left(v_\perp^2+\mathbf{v}_{||}^2\right)/2k_BT}, & \text{if } v_\perp \geq 0; \\ 0, & \text{otherwise.} \end{cases} \tag{A1}$$

The particle, momentum, and energy fluxes associated with (A1) are readily shown to be

$$\phi_\perp = \left(2k_BT/\pi m\right)^{1/2}\ n, \tag{A2}$$

$$M_\perp = nk_BT, \tag{A3}$$

$$Q_\perp = \left(8k_BT/\pi m\right)^{1/2}\ nk_BT, \tag{A4}$$

respectively.

Let n_s^{act} and n_s^{sub} be the number densities of particles of species s leaving the

activating surface and the substrate, respectively. For a nonreactive species such as CO, equating the particle fluxes in the two directions gives, using (A2),

$$n_{\rm CO}^{act}\, T_{act}^{1/2} = n_{\rm CO}^{sub}\, T_{sub}^{1/2}. \tag{A5}$$

Given a total number density $n_{\rm CO}$, the hot and cold populations are

$$\begin{aligned} n_{\rm CO}^{act} &= \frac{T_{sub}^{1/2}}{T_{act}^{1/2} + T_{sub}^{1/2}}\, n_{\rm CO}, \\ n_{\rm CO}^{sub} &= \frac{T_{act}^{1/2}}{T_{act}^{1/2} + T_{sub}^{1/2}}\, n_{\rm CO}. \end{aligned} \tag{A6}$$

The corresponding relations for the reactive species H and H_2 are only slightly more complex. Of the H atoms streaming toward the substrate, a fraction $\gamma_{rec}/2$ undergo abstraction reactions, rebounding as H_2 molecules, and an equal fraction participate in termination reactions, sticking to the substrate. Thus, the remaining fraction $1 - \gamma_{rec}$ of the H atom flux streaming toward the substrate must be balanced by the flux leaving that surface, *viz.*,

$$(1 - \gamma_{rec})\, n_{\rm H}^{act}\, T_{act}^{1/2} = n_{\rm H}^{sub}\, T_{sub}^{1/2}, \tag{A7}$$

whence

$$\begin{aligned} n_{\rm H}^{act} &= \frac{T_{sub}^{1/2}}{(1 - \gamma_{rec})\, T_{act}^{1/2} + T_{sub}^{1/2}}\, n_{\rm H}, \\ n_{\rm H}^{sub} &= \frac{(1 - \gamma_{rec})\, T_{act}^{1/2}}{(1 - \gamma_{rec})\, T_{act}^{1/2} + T_{sub}^{1/2}}\, n_{\rm H}. \end{aligned} \tag{A8}$$

Similarly, the non-dissociating fraction $1 - \gamma_{diss}$ of the H_2 flux approaching the activating wall balances the flux leaving that surface,

$$(1 - \gamma_{diss})\, n_{\rm H_2}^{sub}\, T_{sub}^{1/2} = n_{\rm H_2}^{act}\, T_{act}^{1/2}, \tag{A9}$$

so that

$$n_{H_2}^{act} = \frac{(1-\gamma_{diss})\,T_{sub}^{1/2}}{T_{act}^{1/2} + (1-\gamma_{diss})\,T_{sub}^{1/2}}\; n_{H_2},$$
$$n_{H_2}^{sub} = \frac{T_{act}^{1/2}}{T_{act}^{1/2} + (1-\gamma_{diss})\,T_{sub}^{1/2}}\; n_{H_2}. \qquad \text{(A10)}$$

The H atom flux incident on the substrate is, from (A2),

$$\phi_H = (2k_B T_{act}/\pi m_H)^{1/2}\; n_H^{act}. \qquad \text{(A11)}$$

Substituting from (A8) and introducing the fractional concentrations $X_s = n_s/\Sigma_{s'} n_{s'}$ of species s yields Eq. (6) of §IV.

The relative concentrations of hydrogen atoms and molecules are fixed by noting that the mass flux of H atoms converted to either H_2 molecules or terminated sites at the substrate must balance the mass flux of H_2 molecules dissociating at the activating surface,

$$\gamma_{rec} n_H^{act} (m_H T_{act})^{1/2} = \gamma_{diss} n_{H_2}^{sub} (m_{H_2} T_{sub})^{1/2}. \qquad \text{(A12)}$$

Eq. (10) follows upon substitution of (A8) and (A10) into this result. The gas pressure is determined by computing the total momentum fluxes at either the substrate or the activating wall. From (A3),

$$P = \left(n_H^{act} + n_{H_2}^{act} + n_{CO}^{act}\right) k_B T_{act} + \left(n_H^{sub} + n_{H_2}^{sub} + n_{CO}^{sub}\right) k_B T_{sub}, \qquad \text{(A13)}$$

which reduces to Eq. (7) upon use of (A6), (A8), and (A10). Finally, the energy flux to the substrate and from the activating surface are computed from (A4), with two modifications. First, the excited internal degrees of freedom of the diatomic molecules must be taken into account. At the temperatures of interest in diamond CVD, the rotational modes are fully excited while the vibrational modes are only weakly populated. This enhances the heat flux (A4) by a contribution $\phi_\perp k_B T$, and thus a multiplicative factor of 3/2, for H_2 and CO. For the conductive heat flux we thus obtain

$$q = \left[n_{\rm H}^{act} m_{\rm H}^{-1/2} + \frac{3}{2} n_{\rm H_2}^{act} m_{\rm H_2}^{-1/2} + \frac{3}{2} n_{\rm CO}^{act} m_{\rm CO}^{-1/2} \right] (8/\pi)^{1/2} (k_B T_{act})^{3/2}$$
$$- \left[n_{\rm H}^{sub} m_{\rm H}^{-1/2} + \frac{3}{2} n_{\rm H_2}^{sub} m_{\rm H_2}^{-1/2} + \frac{3}{2} n_{\rm CO}^{sub} m_{\rm CO}^{-1/2} \right] (8/\pi)^{1/2} (k_B T_{sub})^{3/2} . \qquad \text{(A14)}$$

Substituting from (A6), (A8), and (A10) and rearranging using (A11) and (A12) yields Eq. (8) of §IV. Second, the heat of formation of H atoms from H_2 molecules must be taken into account. The resulting recombinative heat flux is just the product of the particle flux $\phi_{\rm H}$, the fraction γ_{rec} of recombining H atoms, and the binding energy per atom, $k_B T_{bind}/2$,

$$q_{rec} = \phi_{\rm H} \gamma_{rec} k_B T_{bind}/2, \qquad \text{(A15)}$$

as given in Eq. (9) of §IV.

2. High-pressure regime

At high gas pressures, the collisional mean free path of the hydrogen atoms and molecules is sufficiently short compared to the separation between the substrate and the activating surface that a hydrodynamic description becomes valid. The continuum transport equations that result are highly nonlinear and generally require the use of numerical methods to obtain a complete solution. Such an approach is much too ambitious for our present purpose. We will content ourselves with an approximate analysis of the H/H_2 system, which nevertheless yields quantitatively useful predictions as well as the correct qualitative trends.

Two features of the high-pressure solutions can be explained by recourse to simple physical arguments. Because the collisions in a gas are predominantly binary interactions, the mean free path of any gas particle – the distance over which it can transport its mass, momentum, or energy – varies inversely with the number density of scattering atoms and molecules. At the same time, the population of transporting particles is directly proportional to the number density. The mass, momentum, or

energy flux carried is determined by the product of these two factors, which is therefore independent of the number density, *i.e.*, of the pressure. This accounts for the observed saturation of the H-atom and heat fluxes at high pressures P. These fluxes are driven by gradients in the macroscopic variables (density, temperature, composition, *etc.*). In the hydrodynamic regime, the gradients are relatively shallow, so that the fluxes are linear in the gradients and thus vary as the inverse first power of the macroscopic scale lengths. This accounts for the observed $1/L$ scaling of the fluxes at high pressures.

In a collisional gas mixture, each species s can acquire a macroscopic diffusion velocity v_s. These velocities are driven by the concentration gradients at a rate determined by the binary diffusion coefficients $D_{s-s'}$ of species s through species s'. They satisfy the Stefan-Maxwell equations [29]

$$\frac{\partial X_s}{\partial x} = \sum_{s'} \frac{X_s X_{s'}}{d_{s-s'}} n \left(v_{s'} - v_s \right), \tag{A16}$$

where the coefficient $d_{s-s'} \equiv n D_{s-s'}$ generally depends upon the temperature but is independent of the number density. For a binary mixture of H atoms and H_2 molecules, Eq. (A16) yields

$$\frac{\partial X_{\rm H}}{\partial x} = \frac{1}{d_{\rm H-H_2}} \left(X_{\rm H} n X_{\rm H_2} v_{\rm H_2} - X_{\rm H_2} n X_{\rm H} v_{\rm H} \right). \tag{A17}$$

In steady state, the particle fluxes must be independent of position and the net mass flux must be zero, whence

$$n X_{\rm H} v_{\rm H} = -2 n X_{\rm H_2} v_{\rm H_2} \equiv -\psi = \text{constant}, \tag{A18}$$

where ψ is the magnitude of the net H atom flux toward the substrate (at $x = 0$). Substituting (A18) into (A17) and using $X_{\rm H_2} = 1 - X_{\rm H}$ gives

$$\frac{\partial X_{\rm H}}{\partial x} = -\frac{\psi}{2 d_{\rm H-H_2}} \left(X_{\rm H} - 2 \right), \tag{A19}$$

whose solution is

$$X_{\mathrm{H}} = 2 - A \exp\left(-x\psi/2d_{\mathrm{H-H_2}}\right). \tag{A20}$$

We have neglected the temperature dependence of $d_{\mathrm{H-H_2}}$ here, and A is a constant to be determined.

It remains to apply boundary conditions to the species concentrations X_s. At sufficiently high pressures, the populations adjacent to the substrate and the activation surface will be completely depleted of H atoms (which recombine) and H_2 molecules (which dissociate), respectively. In the limit, then, we have

$$X_{\mathrm{H}}^{sub} = X_{\mathrm{H}}(0) \rightarrow 0 \quad \Rightarrow \quad A = 2, \tag{A21}$$

$$X_{\mathrm{H}}^{act} = X_{\mathrm{H}}(L) \rightarrow 1 \quad \Rightarrow \quad \psi = \ln 4 \; d_{\mathrm{H-H_2}}/L. \tag{A22}$$

It is crucial to note that ψ is the *net* flux of hydrogen atoms from the activating surface to the substrate. The *total* flux of H atoms striking the substrate, ϕ_{H}, is just the particle flux associated with an isotropic Maxwellian distribution, *viz.*,

$$\phi_{\mathrm{H}} = X_{\mathrm{H}}^{sub} n^{sub} \left(k_B T_{sub}/2\pi m_H\right)^{1/2} = X_{\mathrm{H}}^{sub} P \left(2\pi m_{\mathrm{H}} k_B T_{sub}\right)^{-1/2}. \tag{A23}$$

The net H-atom flux ψ must balance that fraction γ_{rec} of the total flux ϕ_{H} which recombines at the substrate,

$$\psi = \gamma_{rec} \phi_{\mathrm{H}}. \tag{A24}$$

Combining (A24) and (A22), and averaging the diffusion coefficient at the substrate and activating temperatures to approximately account for its temperature dependence, we obtain

$$\phi_{\mathrm{H}} \approx \ln 2 \left(d_{\mathrm{H-H_2}}^{act} + d_{\mathrm{H-H_2}}^{sub}\right) / \gamma_{rec} L \tag{A25}$$

for the total atomic hydrogen flux to the substrate.

Results (A23) and (A25) can be combined to yield

$$X_{\mathrm{H}}^{sub} \approx (2\pi m_{\mathrm{H}} k_B T_{sub})^{1/2} \frac{\ln 2}{\gamma_{rec}} \frac{d_{\mathrm{H-H_2}}^{act} + d_{\mathrm{H-H_2}}^{sub}}{L} \frac{1}{P}. \tag{A26}$$

Thus, $X_{\mathrm{H}}^{sub} \propto P^{-1} \rightarrow 0$ as the pressure increases, as asserted above. The net H_2 flux to the activating surface, $\psi/2$, is related to the total flux $\phi_{\mathrm{H_2}}$ by

$$\psi/2 = \gamma_{diss} \phi_{\mathrm{H_2}}, \tag{A27}$$

whence

$$X_{\mathrm{H_2}}^{act} \approx (2\pi m_{\mathrm{H_2}} k_B T_{act})^{1/2} \frac{\ln 2}{2\gamma_{diss}} \frac{d_{\mathrm{H-H_2}}^{act} + d_{\mathrm{H-H_2}}^{sub}}{L} \frac{1}{P}. \tag{A28}$$

Consequently, $X_{\mathrm{H_2}}^{act} \propto P^{-1} \rightarrow 0$ at high pressures, as well.

The total energy flux is composed of two terms: the familiar conductive component given by Fourier's law, *i.e.*, the product of the temperature gradient and the thermal conductivity of the gas; and a contribution due to the flow of enthalpy at the species' diffusion velocities. Thus,

$$q_{tot} = -\kappa \frac{\partial T}{\partial x} + \sum_s n X_s v_s h_s, \tag{A29}$$

where the specific enthalpies are $h_{\mathrm{H}} = k_B T_{bind}/2 + 5k_B T/2$ and $h_{\mathrm{H_2}} = 7k_B T/2$ for atomic and molecular hydrogen, respectively. The recombinative heat flux computed in the DSMC model is just the contribution due to the heat of formation of H from H_2, whence

$$q_{rec} = \phi_{\mathrm{H}} \gamma_{rec} k_B T_{bind}/2. \tag{A30}$$

The remaining terms in (A29) constitute the conductive heat flux as calculated by the DSMC model. For a gas mixture such as H/H_2, the thermal conductivity κ is a summation of the conductivities of the individual constituents. Each such contribution is weighted by that species' concentration and reduced by a factor accounting for binary collisions with other species present in the mixture [29]. Also, the individual

conductivities vary with temperature. We avoid these complexities by using the mean of the conductivities at the substrate and activating temperatures, and the average temperature gradient across the system, to estimate the heat flux. As noted above, at high pressures the composition tends toward 100% H atoms at the activating surface and 100% H_2 molecules at the substrate. Then the conductive heat flux can be approximated as

$$q_{cond} \approx \left(\kappa_{\mathrm{H}}^{act} + \kappa_{\mathrm{H}_2}^{sub}\right)\left(T_{act} - T_{sub}\right)/2L + 3\phi_{\mathrm{H}}\gamma_{rec}k_B\left(T_{act} + T_{sub}\right)/8, \qquad \text{(A31)}$$

as given in Eq. (16) in §4. Here, we have used the average of the activating and substrate temperatures to estimate the enthalpic contribution $\phi_{\mathrm{H}}\gamma_{rec}3k_BT/4$ to the conductive flux.

TABLES

TABLE 1. Parameters for the variable soft-sphere collision model: d is the molecular diameter, T^{ref} the reference temperature, ω the viscosity index, α the scattering parameter, m the molecular mass, and Z^{rot} the rotational relaxation number. Values were taken from Bird [3] where available. The values of ω and α for atomic hydrogen were set equal to those for helium. The diameter for atomic hydrogen and the rotational relaxation numbers for molecular hydrogen and carbon monoxide were taken from the Sandia transport data base [19]. The parameters C_1 and C_2 for the temperature dependence of the vibrational relaxation number ($Z_v = (C_1/T^{\omega})\exp(C_2 T^{-1/3})$) were set to 9.1 and 220.0, respectively, for all collisions involving H_2.

species	d (Å)	T^{ref} (K)	ω	α	m (amu)	$Z^{rot}(298)$
H_2	2.88	273	0.67	1.35	2	280.0
CO	4.12	273	0.73	1.49	28	1.8
H	2.05	273	0.66	1.26	1	—

TABLE 2. Comparison between free-streaming analytic (indicated by superscript FS) and low-pressure DSMC results for H/H_2 mixtures. The conductive (q_{cond}) and recombinative (q_{rec}) heat fluxes are in W cm^{-2}. L is the separation between the substrate and activating surface, P is the pressure, and X_H is the atomic hydrogen mole fraction. X_H^{DSMC} was evaluated by averaging X_H at the bounding surfaces. In all cases, the spatial variation in X_H was less than 2%.

L (cm)	P (Torr)	q_{cond}^{DSMC}	q_{cond}^{FS}	q_{rec}^{DSMC}	q_{rec}^{FS}	X_{H}^{DSMC}	X_{H}^{FS}
0.25	0.043	1.63	1.65	0.89	0.89	0.965	0.967
0.5	0.045	1.65	1.73	0.95	0.94	0.965	0.967
1.0	0.050	1.74	1.93	1.09	1.04	0.960	0.967

TABLE 3. Comparison between analytic hydrodynamic (indicated by superscript HD) and high-pressure DSMC results for H/H_2 mixtures. The conductive (q_{cond}) and recombinative (q_{rec}) heat fluxes are in W cm^{-2}, and the atomic hydrogen fluxes to the substrate are in 10^{19} atoms cm^{-2} s^{-1}. L is the separation between the substrate and activating surface and P is the pressure.

L (cm)	P (Torr)	q_{cond}^{DSMC}	q_{cond}^{HD}	q_{rec}^{DSMC}	q_{rec}^{HD}	ϕ_{H}^{DSMC}	ϕ_{H}^{HD}
0.25	26.2	90.1	128.	279.	400.	1052.	1520.
0.5	25.0	48.3	56.	175.	200.	660.	760.
1.0	24.2	25.9	28.	101.	100.	381.	380.

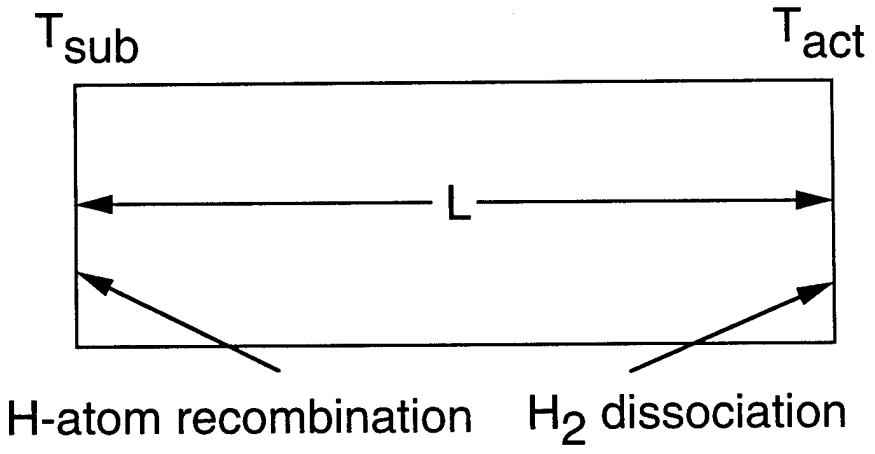

FIG. 1. Computational domain used for the DSMC calculations.

FIG. 2. (a)

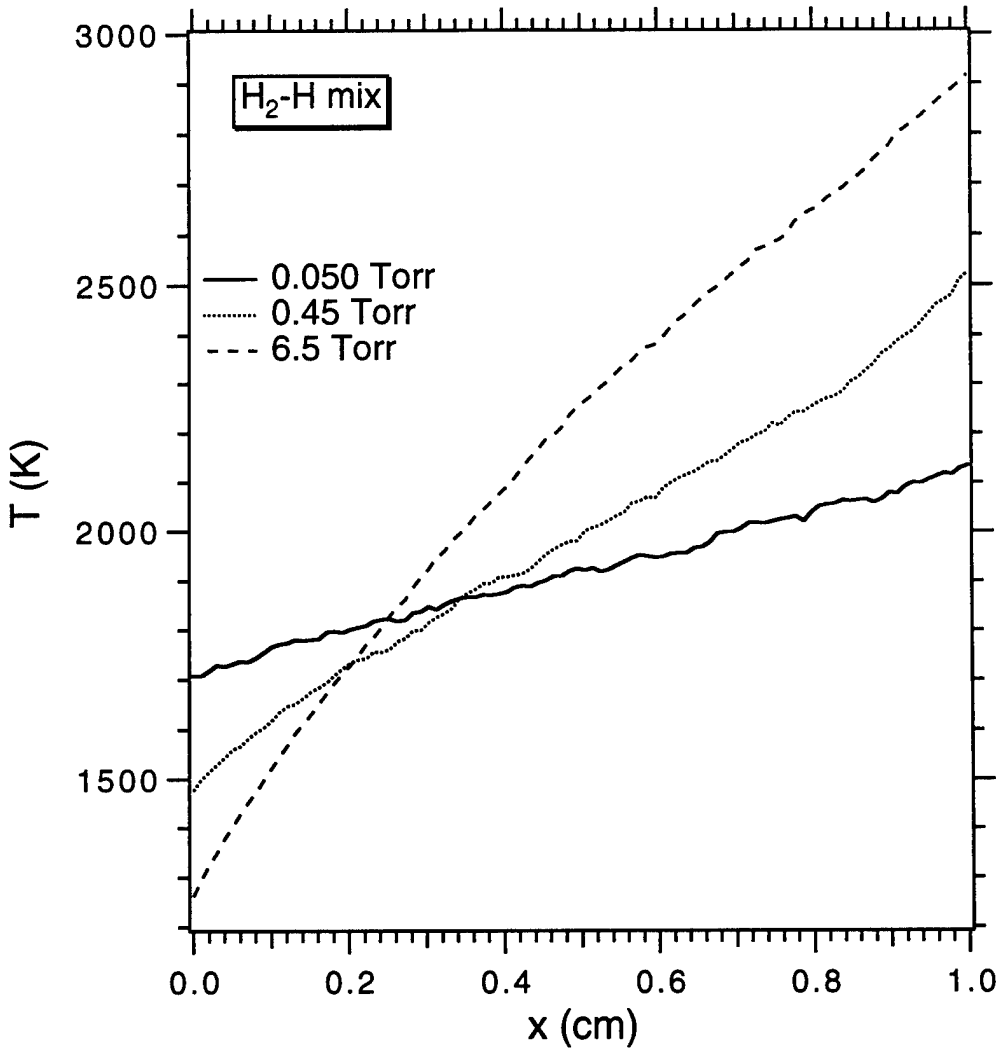

FIG. 2. Spatially resolved (a) temperature and (b) species profiles for H/H_2 mixtures. The diamond substrate at 1200 K is located at $x = 0$, and the activating surface, located at $x = 1$ cm, is maintained at 3000 K. Surface reaction probabilities are those of Brenner *et al.* and 100% hydrogen dissociation at the activating surface is assumed.

FIG. 2. (b)

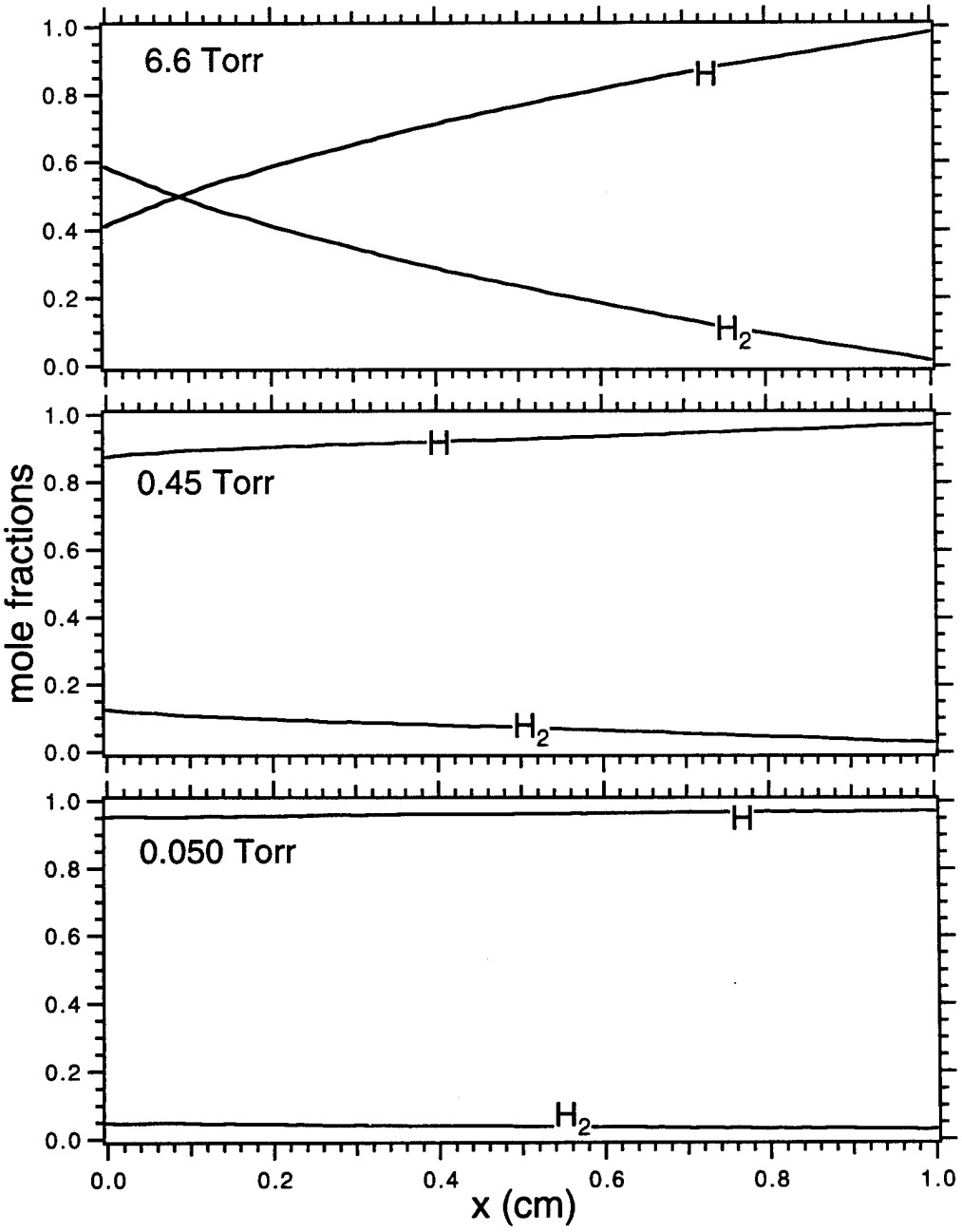

FIG. 2. Spatially resolved (a) temperature and (b) species profiles for H/H_2 mixtures. The diamond substrate at 1200 K is located at $x = 0$, and the activating surface, located at $x = 1$ cm, is maintained at 3000 K. Surface reaction probabilities are those of Brenner *et al.* and 100% hydrogen dissociation at the activating surface is assumed.

FIG. 3. (a)

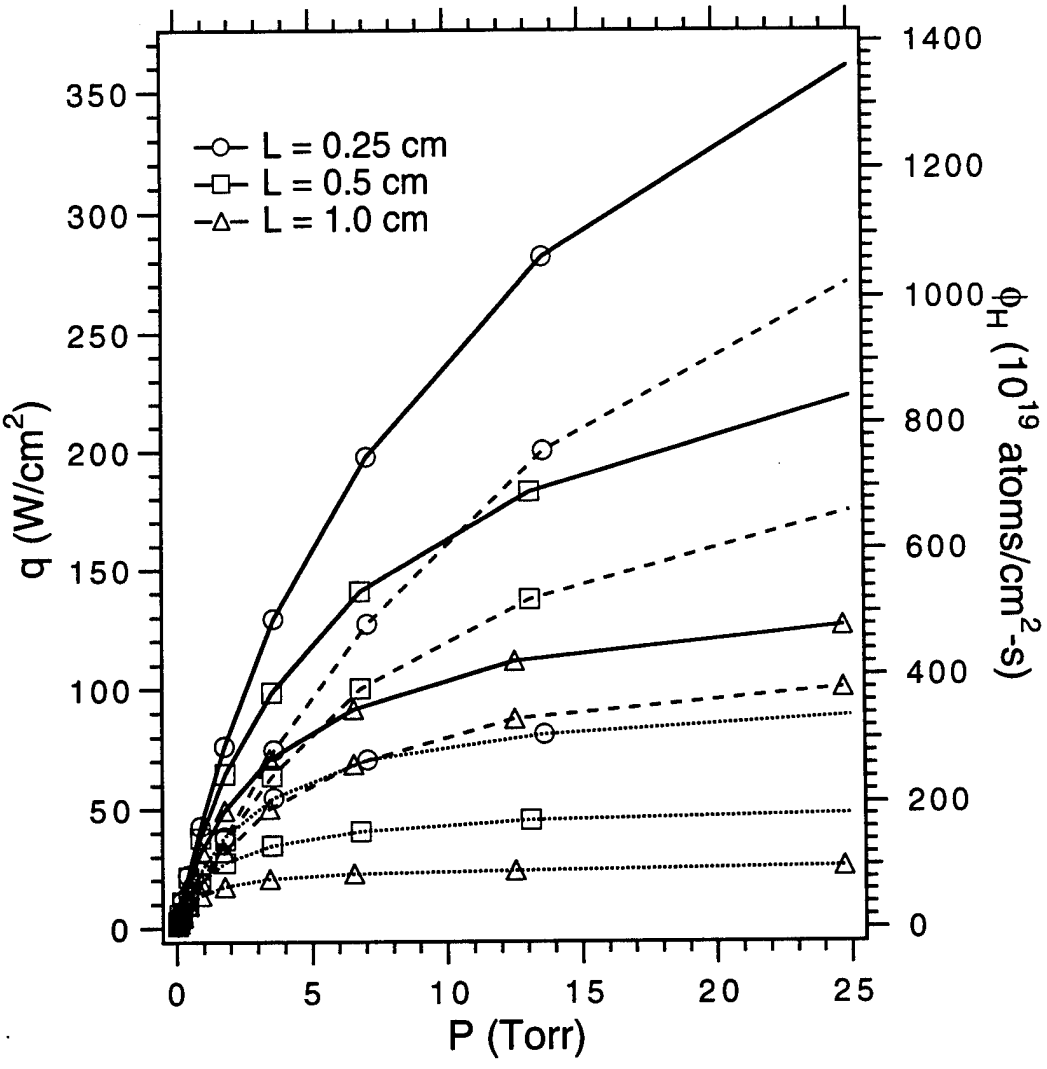

FIG. 3. Pressure dependence of q_{cond} (dotted lines), q_{rec} (dashed lines), and q_{tot} (solid lines) for H/H_2 mixture at various values of the substrate-heat source separation. The hydrogen atom flux, ϕ_H (dashed lines), is exactly proportional to q_{rec} and is plotted against the right axis. Figure 3b is a blow up of the low-pressure region of Fig. 3a.

FIG. 3. (b)

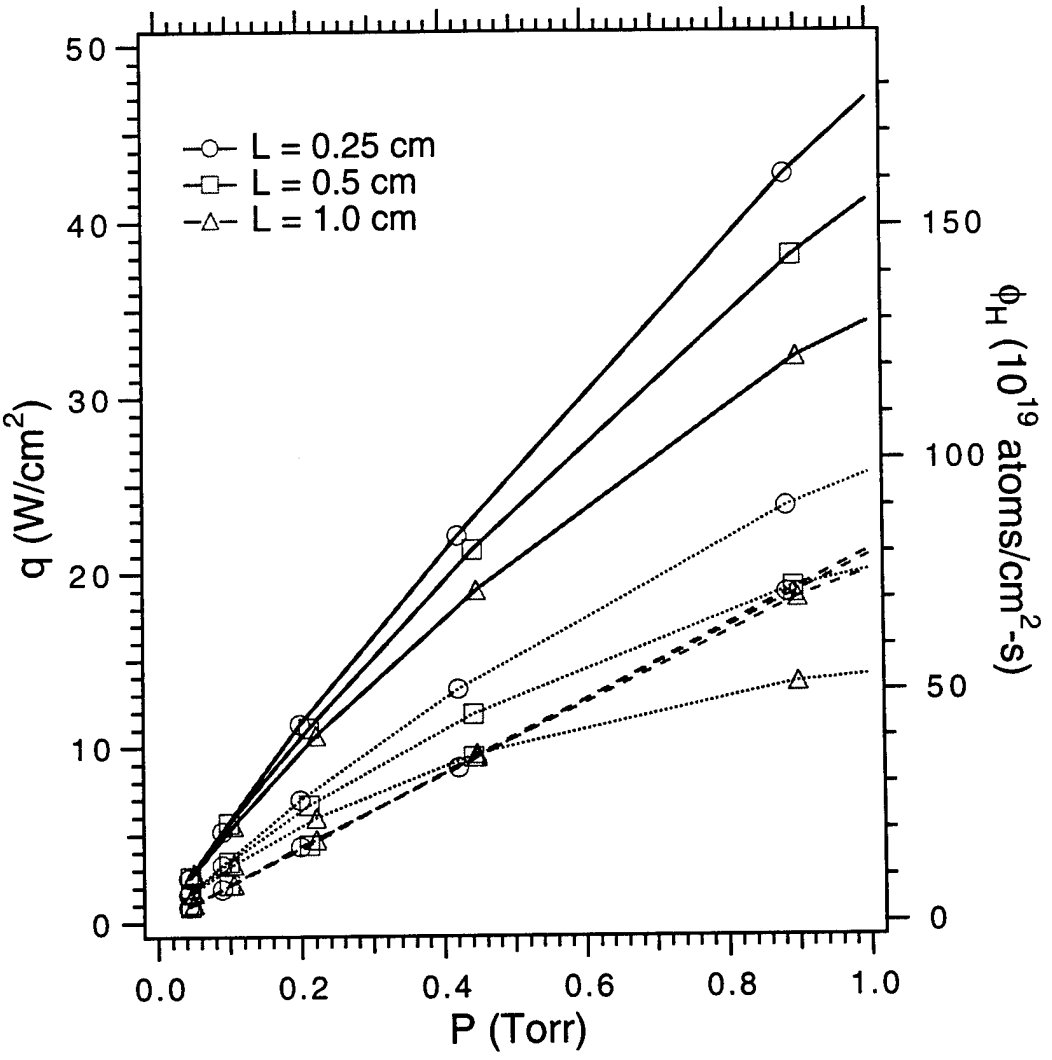

FIG. 3. Pressure dependence of q_{cond} (dotted lines), q_{rec} (dashed lines), and q_{tot} (solid lines) for H/H_2 mixture at various values of the substrate-heat source separation. The hydrogen atom flux, ϕ_H (dashed lines), is exactly proportional to q_{rec} and is plotted against the right axis. Figure 3b is a blow up of the low-pressure region of Fig. 3a.

FIG. 4. (a)

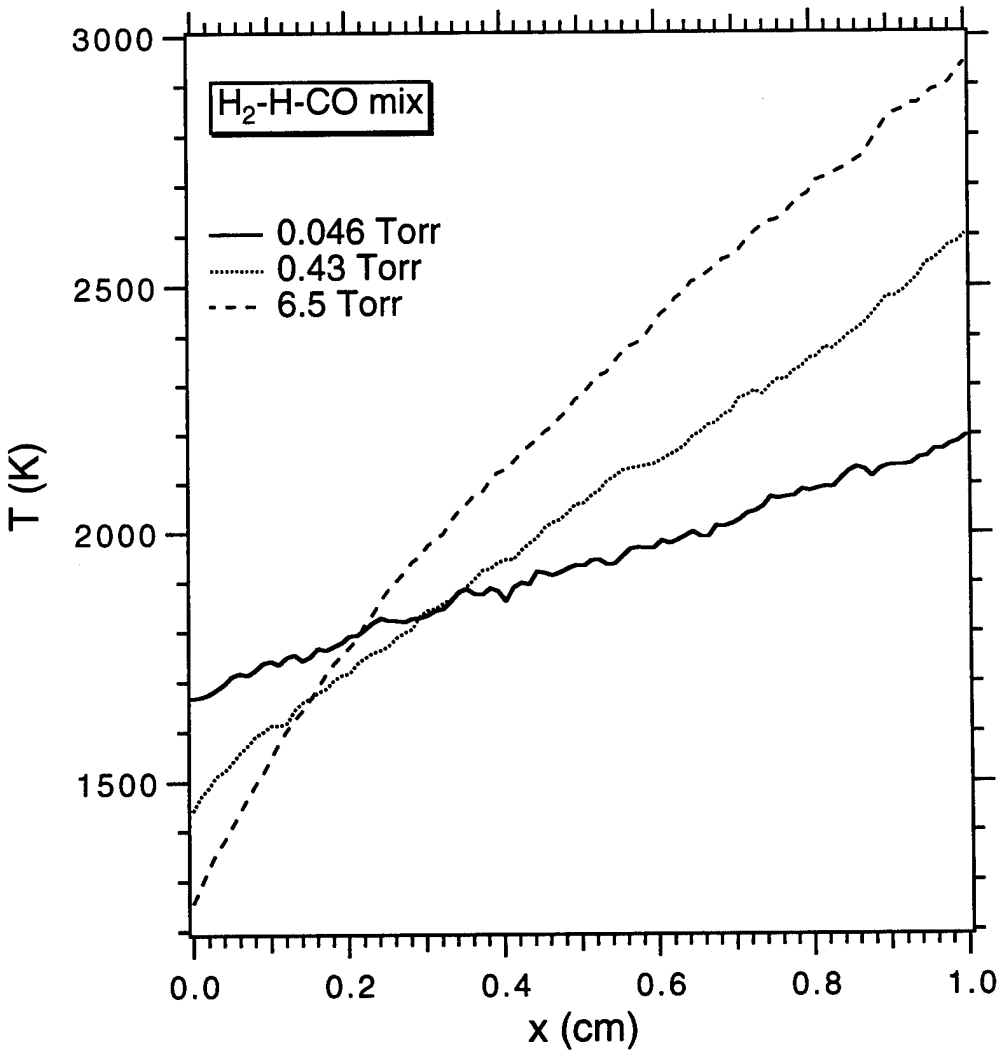

FIG. 4. Spatially resolved (a) temperature and (b) species profiles for $H/H_2/CO$ mixtures. The diamond substrate at 1200 K is located at $x = 0$; the activating surface, located at $x = 1$ cm, is maintained at 3000 K. Surface reaction probabilities are those of Brenner *et al.* and 100% hydrogen dissociation at the activating surface is assumed.

FIG. 4. (b)

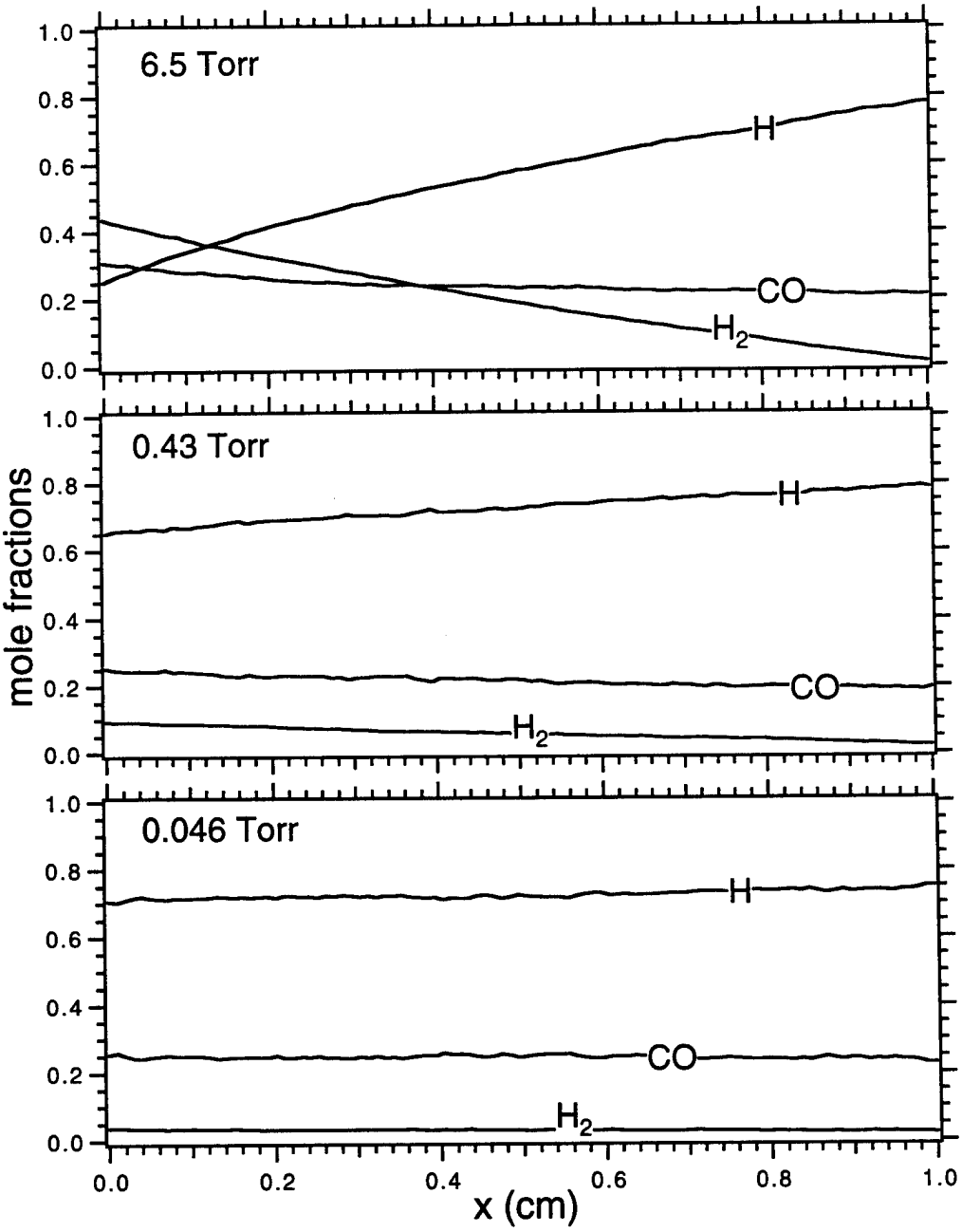

FIG. 4. Spatially resolved (a) temperature and (b) species profiles for $H/H_2/CO$ mixtures. The diamond substrate at 1200 K is located at $x = 0$; the activating surface, located at $x = 1$ cm, is maintained at 3000 K. Surface reaction probabilities are those of Brenner *et al.* and 100% hydrogen dissociation at the activating surface is assumed.

FIG. 5. (a)

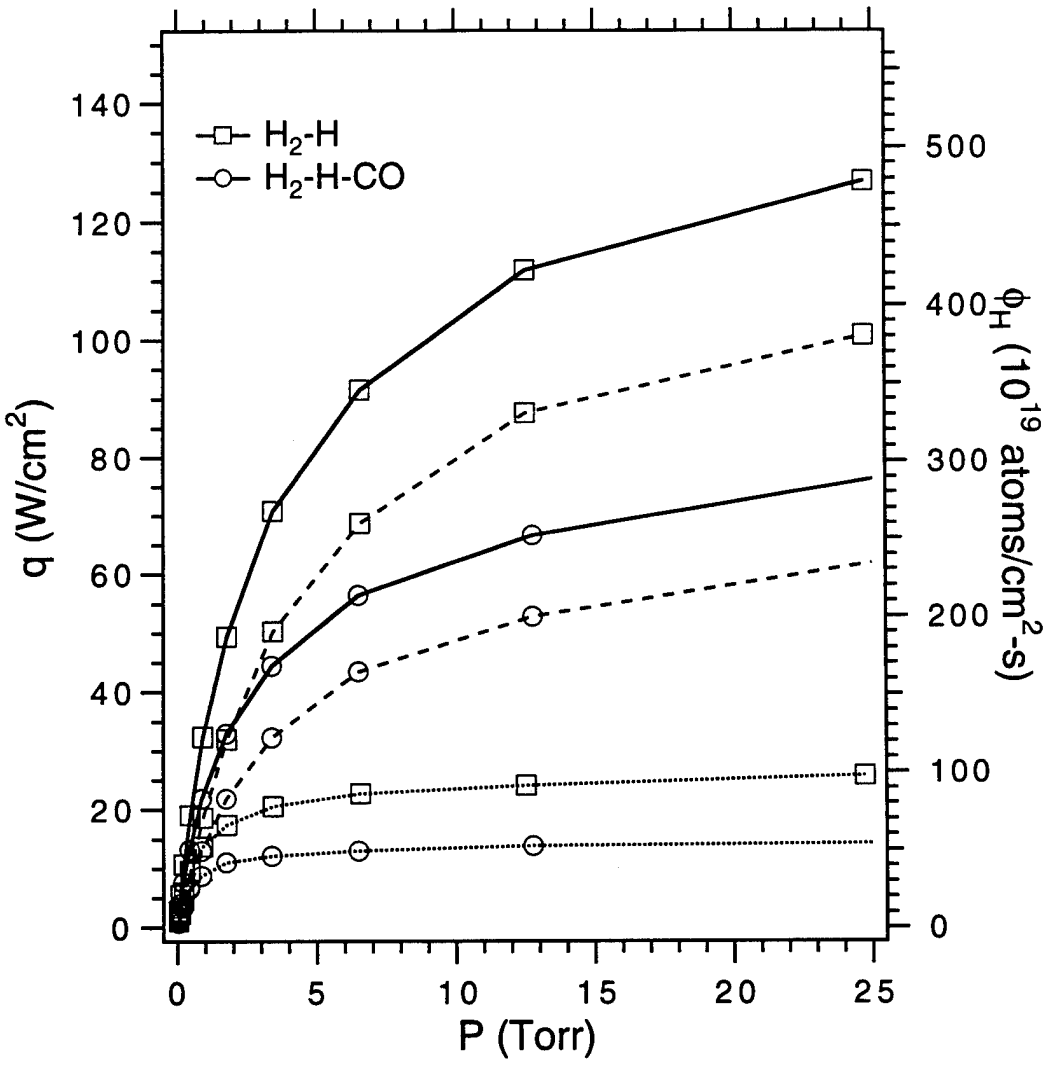

FIG. 5. Comparison of the pressure dependence of q_{cond} (dotted lines), q_{rec} (dashed lines), and q_{tot} (solid lines) for H/H_2 and $H/H_2/CO$ mixtures. L is 1 cm. The hydrogen atom flux, ϕ_H (dashed lines), is exactly proportional to q_{rec} and is plotted against the right axis. Figure 5b is a blow up of the low-pressure region of Fig. 5a.

FIG. 5. (b)

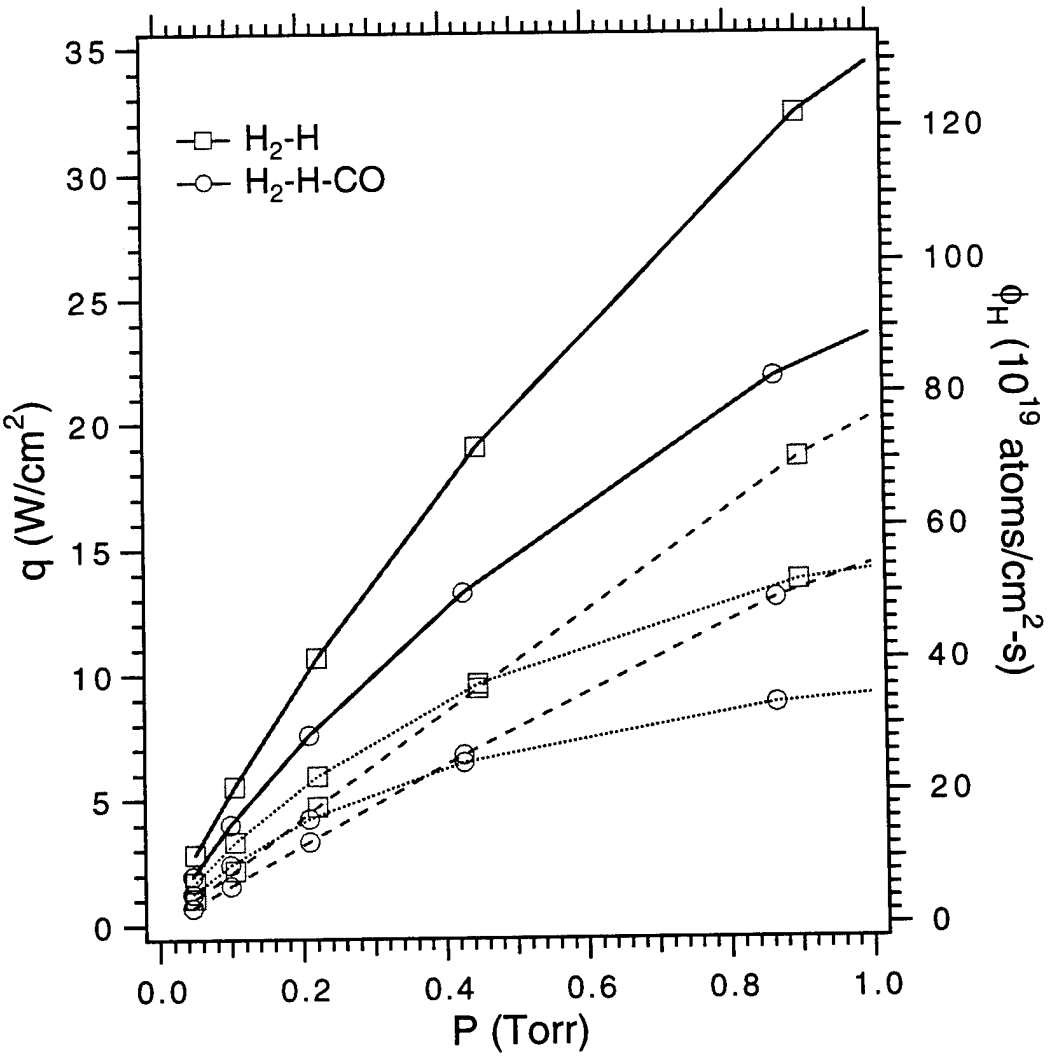

FIG. 5. Comparison of the pressure dependence of q_{cond} (dotted lines), q_{rec} (dashed lines), and q_{tot} (solid lines) for H/H_2 and $H/H_2/CO$ mixtures. L is 1 cm. The hydrogen atom flux, ϕ_H (dashed lines), is exactly proportional to q_{rec} and is plotted against the right axis. Figure 5b is a blow up of the low-pressure region of Fig. 5a.

FIG. 6. (a)

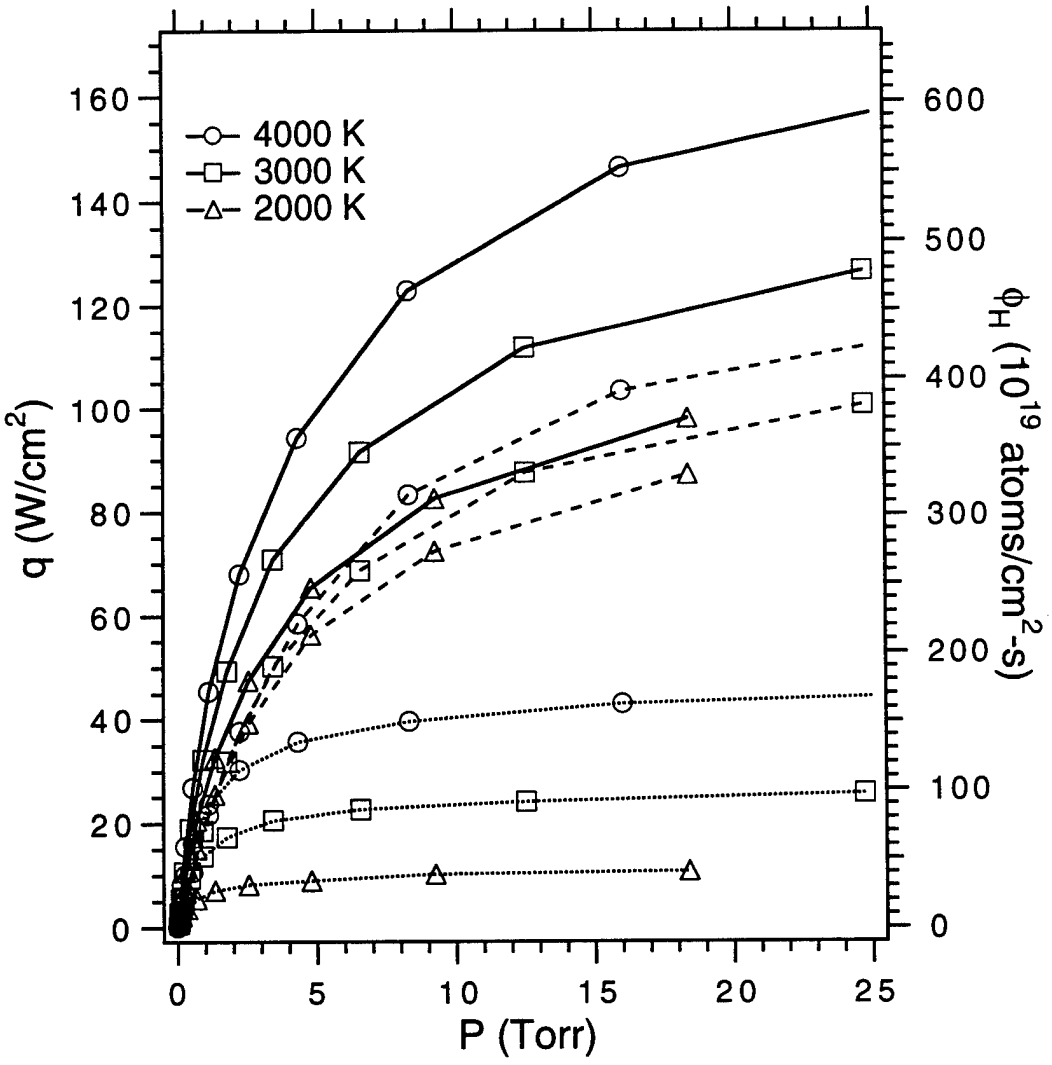

FIG. 6. Pressure dependence of q_{cond} (dotted lines), q_{rec} (dashed lines), and q_{tot} (solid lines) for H/H_2 mixtures for various values of the temperature at the activating surface. L is 1 cm. The hydrogen atom flux, ϕ_H (dashed lines), is exactly proportional to q_{rec} and is plotted against the right axis. Figure 6b is a blow up of the low-pressure region of Fig. 6a.

FIG. 6. (b)

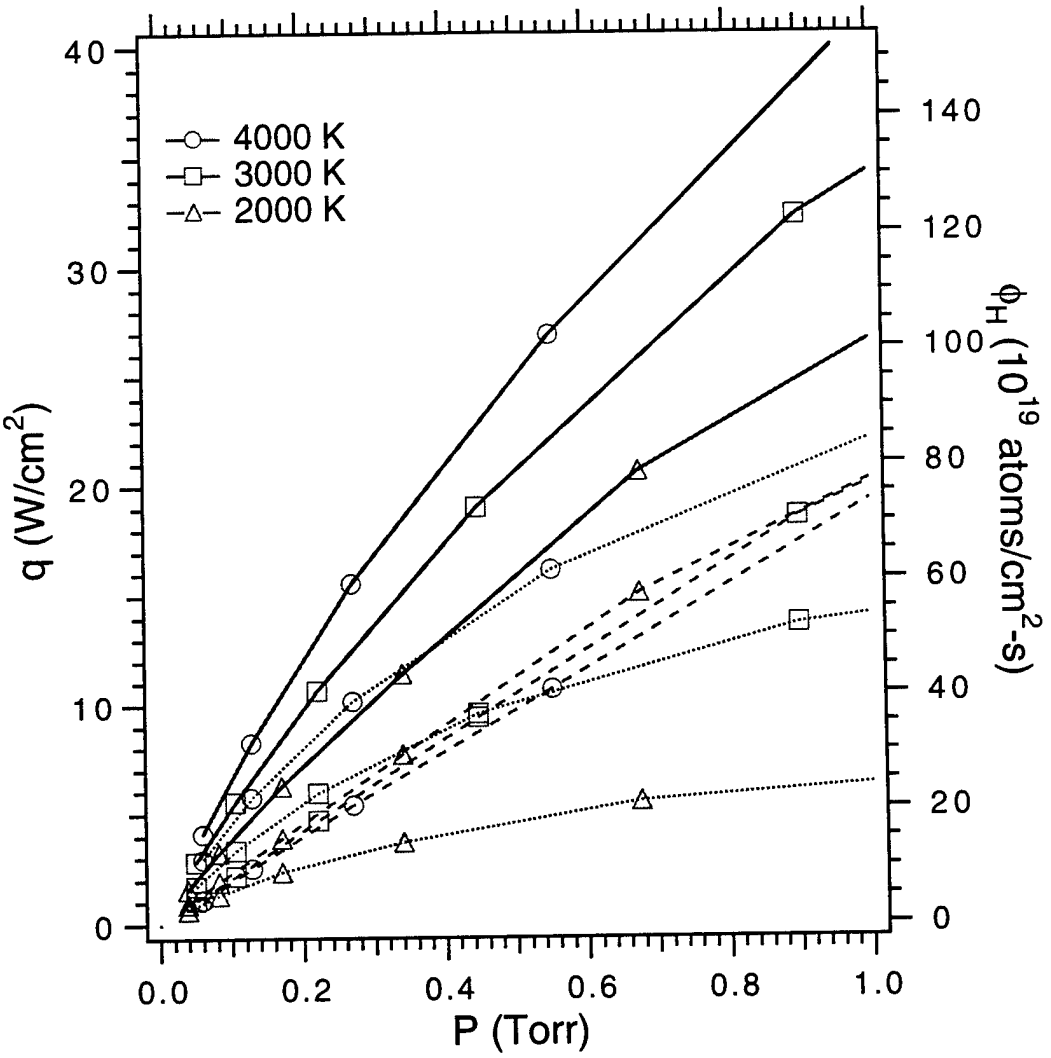

FIG. 6. Pressure dependence of q_{cond} (dotted lines), q_{rec} (dashed lines), and q_{tot} (solid lines) for H/H_2 mixtures for various values of the temperature at the activating surface. L is 1 cm. The hydrogen atom flux, ϕ_H (dashed lines), is exactly proportional to q_{rec} and is plotted against the right axis. Figure 6b is a blow up of the low-pressure region of Fig. 6a.

FIG. 7. (a)

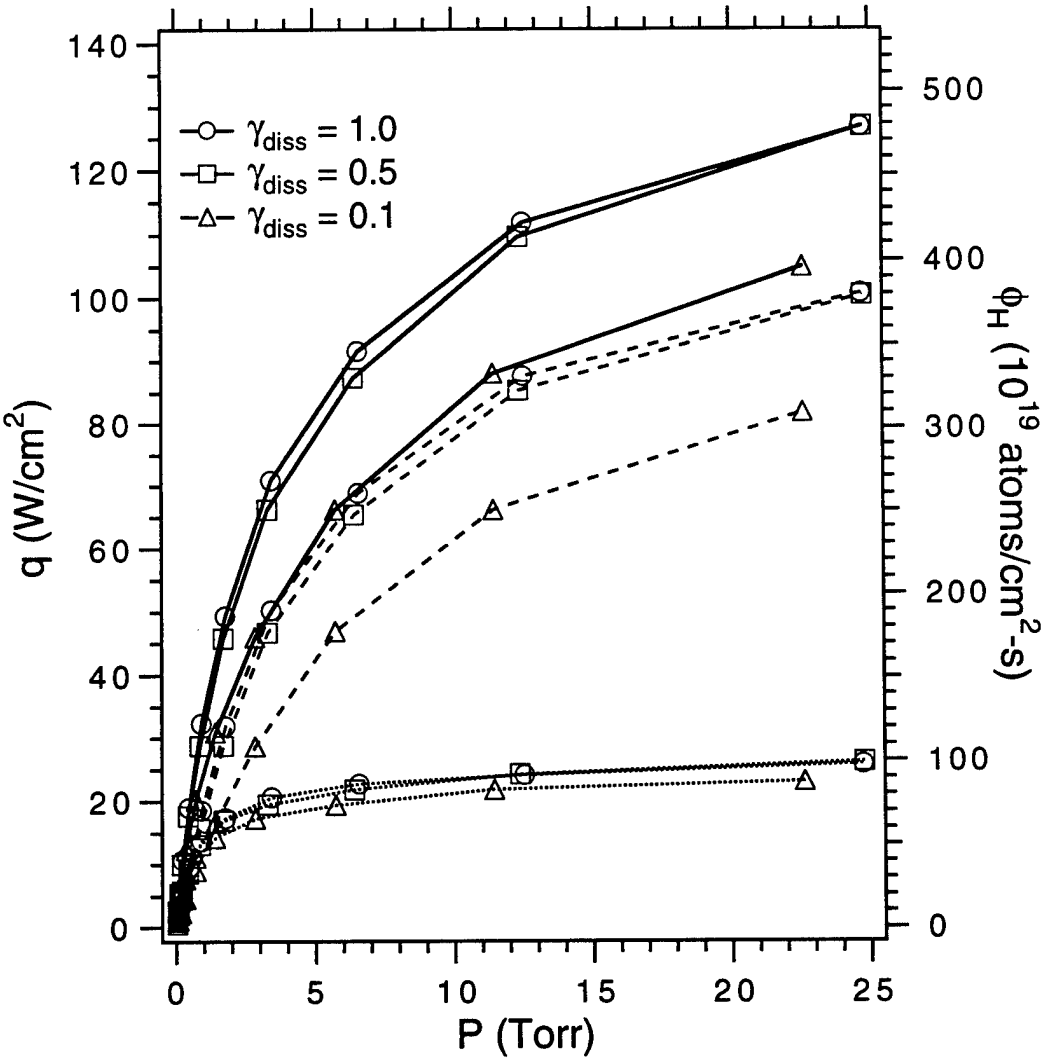

FIG. 7. Pressure dependence of q_{cond} (dotted lines), q_{rec} (dashed lines), and q_{tot} (solid lines) for H/H_2 mixtures at various values of the hydrogen dissociation probability. L is 1 cm. The hydrogen atom flux, ϕ_H (dashed lines), is exactly proportional to q_{rec} and is plotted against the right axis. Figure 7b is a blow up of the low-pressure region of Fig. 7a.

FIG. 7. (b)

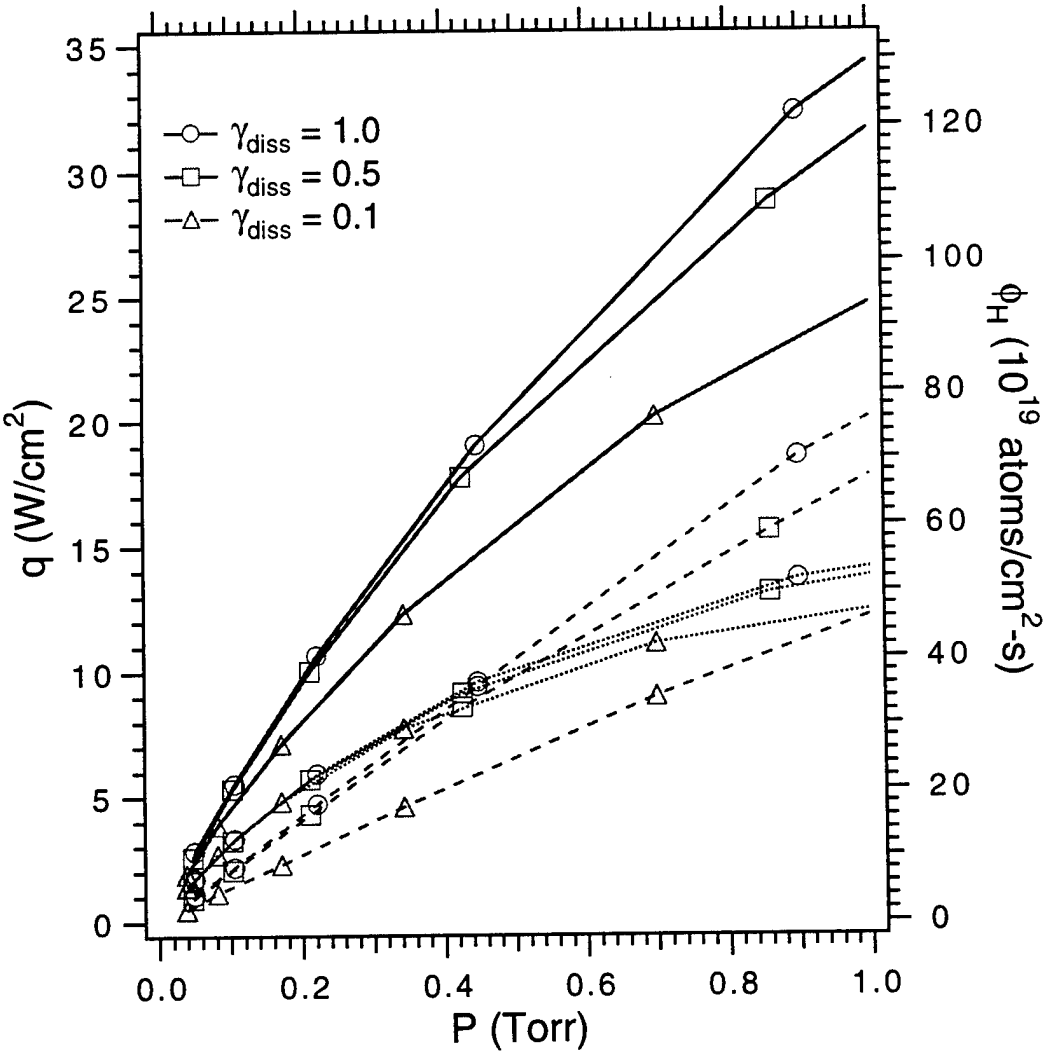

FIG. 7. Pressure dependence of q_{cond} (dotted lines), q_{rec} (dashed lines), and q_{tot} (solid lines) for H/H_2 mixtures at various values of the hydrogen dissociation probability. L is 1 cm. The hydrogen atom flux, ϕ_H (dashed lines), is exactly proportional to q_{rec} and is plotted against the right axis. Figure 7b is a blow up of the low-pressure region of Fig. 7a.

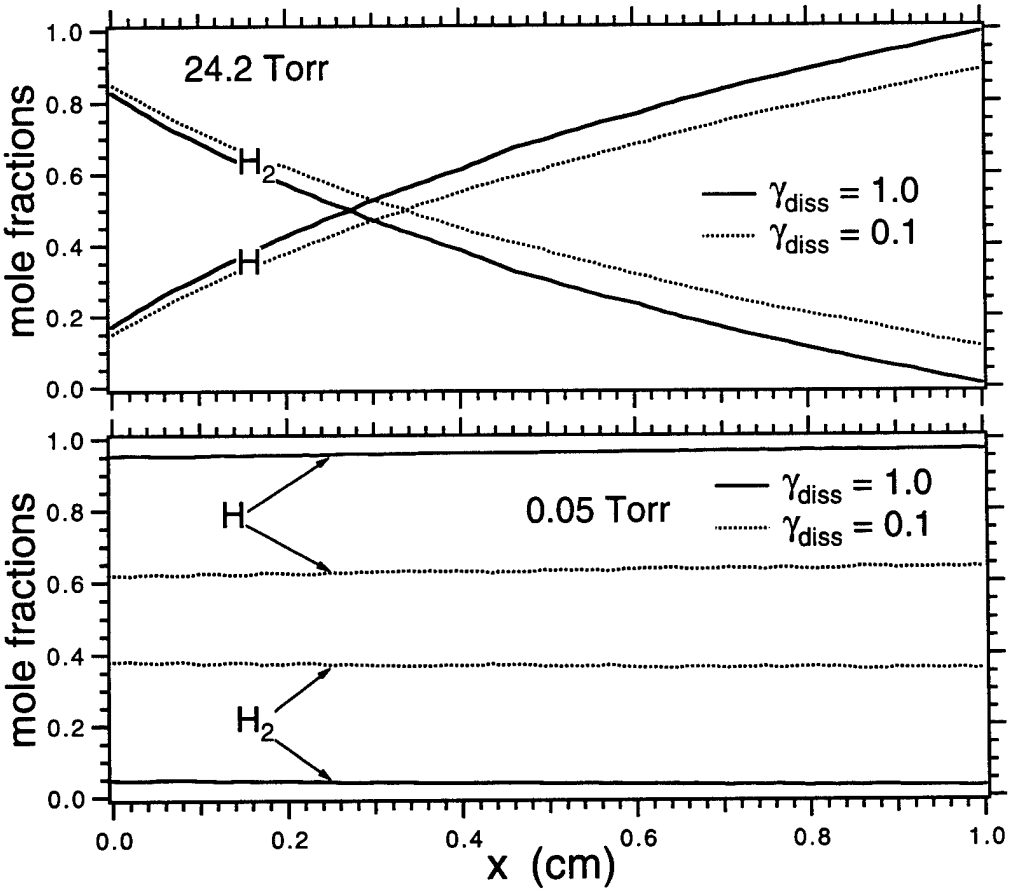

FIG. 8. Spatially resolved species profiles for H/H_2 mixtures with hydrogen dissociation probabilities of 100% and 10% at the activating surface. The diamond substrate at 1200 K is located at $x = 0$; the activating surface, located at $x = 1$ cm, is maintained at 3000 K.

FIG. 9. (a)

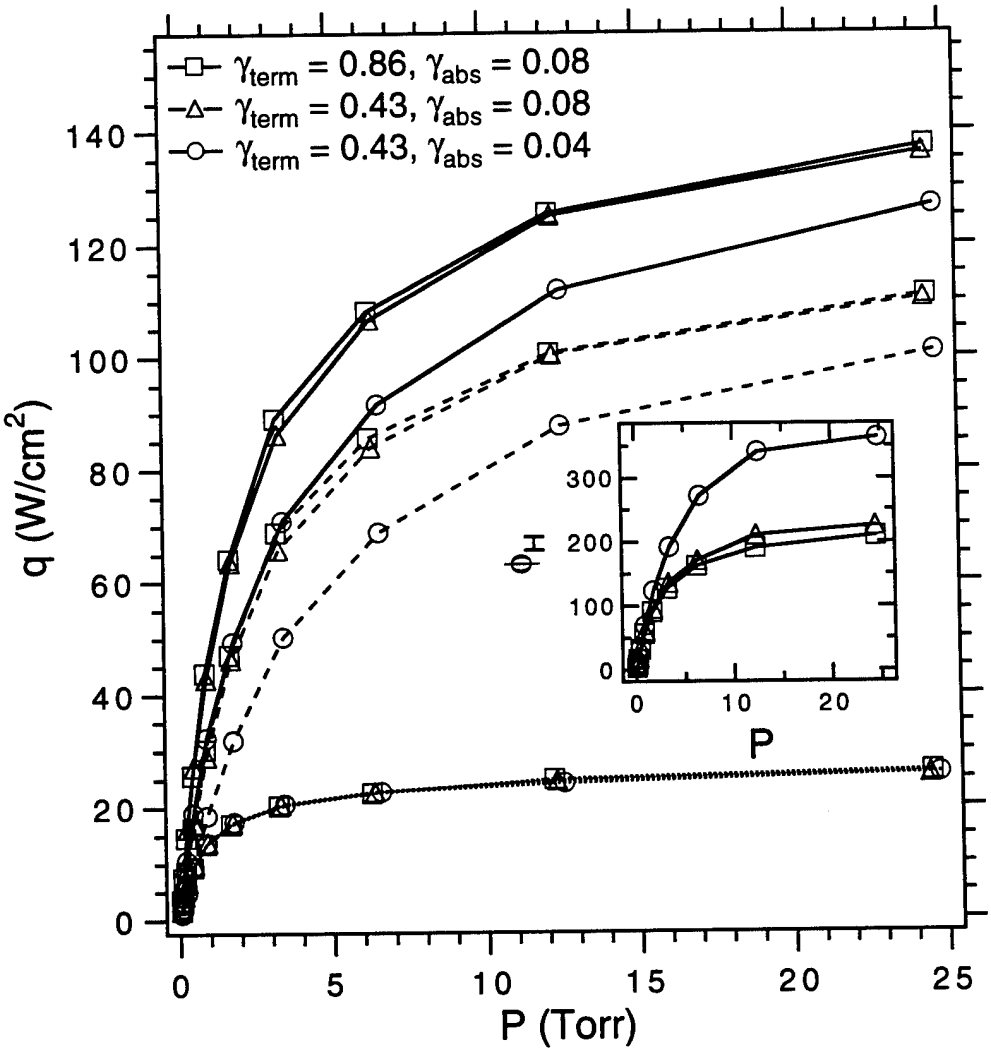

FIG. 9. Pressure dependence of q_{cond} (dotted lines), q_{rec} (dashed lines), and q_{tot} (solid lines) for H/H_2 mixtures for three sets of the surface reaction probabilities. L is 1 cm. The hydrogen atom flux, ϕ_H (dashed lines), is exactly proportional to q_{rec} and is plotted against the right axis. Figure 9b is a blow up of the low-pressure region of Fig. 9a.

FIG. 9. (b)

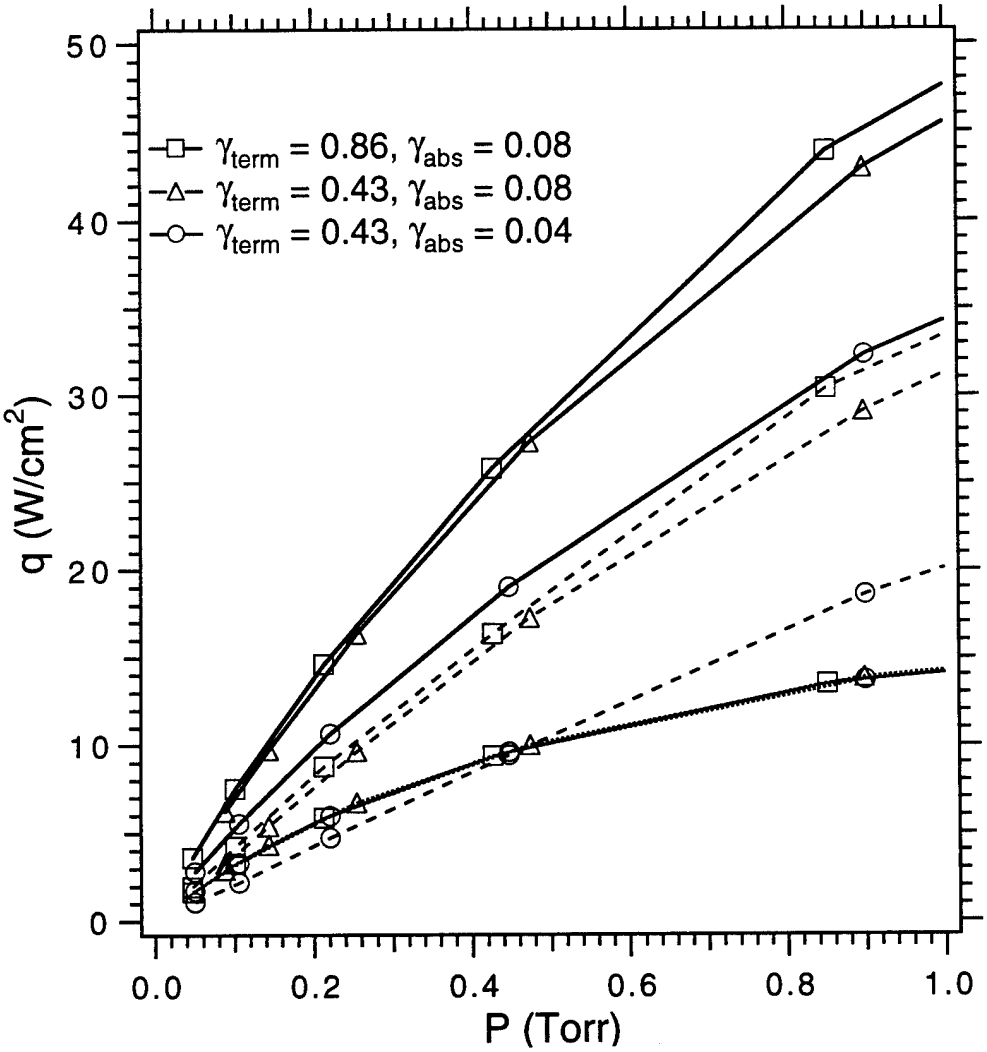

FIG. 9. Pressure dependence of q_{cond} (dotted lines), q_{rec} (dashed lines), and q_{tot} (solid lines) for H/H_2 mixtures for three sets of the surface reaction probabilities. L is 1 cm. The hydrogen atom flux, ϕ_H (dashed lines), is exactly proportional to q_{rec} and is plotted against the right axis. Figure 9b is a blow up of the low-pressure region of Fig. 9a.